

國立交通大學

電子工程學系 電子研究所碩士班

碩士論文

正交分頻多工通信系統於時變與多重路徑衰減  
通道之通道估測與訊號偵測設計

**Design of Channel Estimation and Data Detection for  
OFDM Systems in Time-varying and Multipath  
Fading Channels**

研究生：蔡金融

指導教授：陳紹基 博士

中華民國九十五年七月

正交分頻多工通信系統於時變與多重路徑衰減通道之  
通道估測與訊號偵測設計

**Design of Channel Estimation and Data Detection for OFDM  
Systems in Time-varying and Multipath Fading Channels**

研究生：蔡金融

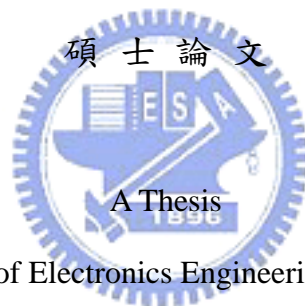
Student : Chin-Jung Tsai

指導教授：陳紹基 博士

Advisor : Sau-Gee Chen

國立交通大學

電子工程學系 電子研究所碩士班



Submitted to Department of Electronics Engineering & Institute of Electronics

College of Electrical and Computer Engineering

National Chiao Tung University

in Partial Fulfillment of the Requirements

for the Degree of

Master

in

Electronics Engineering

July 2006

Hsinchu, Taiwan, Republic of China

中華民國九十五年七月

# 正交分頻多工通信系統於時變與多重路徑衰減通道之通道估測與訊號偵測設計


學生：蔡金融

指導教授：陳紹基 博士

國立交通大學

電子工程學系 電子研究所碩士班

## 摘 要



在本篇論文中，探討了數種正交多工分頻系統於時變與多重路徑衰減通道的通道估測與訊號偵測技術。在單個正交多工分頻系統符元內的通道變化，將會破壞次載波彼此間的正交性，而其所造成次載波間的干擾會使系統效能下降。此效能誤差量將會隨著移動的速度、載波頻率或是符元的持續時間增加而變的嚴重。基於現有的通道估測與訊號偵測方法，我們提出了一些改進的方式。所提出的訊號偵測方法利用了時變通道內隱含的時間多樣性，而不是只將其視為次載波間的干擾。它的效能較一般次載波干擾消去法優異，並且擁有可接受的複雜度。而所提出的通道估測方法基於適當的數學模型假設。此數學模型可以有效減少所需估計的參數，使估測可行並且更為精準。

# **Design of Channel Estimation and Data Detection for OFDM Systems in Time-varying and Multipath Fading Channels**

Student: Chin-Jung Tsai

Advisor: Sau-Gee Chen

Department of Electronics Engineering & Institute of Electronics  
National Chiao Tung University

## **Abstract**

In this thesis, several methods for channel estimation and data detection of OFDM systems in time-varying and multipath fading channels are investigated. Channel variations over an OFDM symbol destroy the orthogonality between subcarriers. The corresponding intercarrier-interference (ICI) degrades the system performance. This error floor becomes more severe as mobile speed, carrier frequency, or symbol duration increases. Based on the existing channel estimation methods and the data detection methods, several modifications to improve the system performances or to reduce the system computational complexities are proposed. The proposed data detection methods exploit time diversity involved in the nature of the time-varying channels. Thus, the proposed methods outperform the conventional methods, like ICI cancellation method and least square (LS) detection. For implementation, the proposed methods are modified to have acceptable complexities. The proposed channel estimation methods are based on appropriate mathematical models. The estimated parameters can be reduced by using these mathematical models. Therefore, channel estimation in fast fading channels becomes feasible and trackable.

## 誌 謝

首先要感謝我的指導教授 陳紹基博士。當我遇到研究上的疑惑與困難時，能適時的給予指導以及提供思考方向，使我能順利的完成本篇論文，而在生活上老師也提供了很多幫助與寶貴的經驗，在此致上由衷的感謝。

在碩士生涯的兩年中，我也要感謝實驗室的夥伴文威、敏杰、譽桀、昀震、彥欽和聖國在生活上的幫助與關心，而跟你們研究上的討論，使我獲益良多。和你們同窗的這段時間也讓我了解到需要學習的事情還很多。另外要特別感謝曲建全學長在研究上與生活上的幫助。能夠在這間實驗室和各位一同奮鬥、歡笑真的覺得很幸運，祝各位將來一切順利。

最後感謝我的父母與家人，從小以來對我的呵護與栽培，讓我能順利完成學業，並且擁有寶貴的人生經歷，在此獻上無限的感激與敬意。





# Contents

---

中文摘要	i
<b>Abstract</b>	<b>ii</b>
誌謝	<b>iii</b>
<b>Content</b>	<b>v</b>
<b>List of Tables</b>	<b>ix</b>
<b>List of Figures</b>	<b>x</b>
<b>Chapter 1 Introduction</b>	<b>1</b>
1.1 Background and Motivation	2
1.2 Organization of the Thesis	4
<b>Chapter 2 Fundamentals of OFDM Systems</b>	<b>6</b>
2.1 OFDM System Model	7
2.1.1 Continuous-time Model	7
2.1.2 Discrete-time Model	9
2.2 Channel Characteristics in Wireless Communication Environments	10
2.3 Analysis of Intercarrier Interference	13
<b>Chapter 3 Investigation of Existing Data Detection and Channel Estimation Methods</b>	<b>17</b>
3.1 Existing Data Detection Methods	18
3.1.1 Single-tap Equalization	18
3.1.2 Least-square Detection (Decorrelating Detection)	18
3.1.3 Jeon's Method of Least-square Detection	19
3.1.4 Intercarrier Interference Cancellation	21
3.1.5 Choi's Method of Successive Detection	22
3.1.6 Simulation Results	25

---

3.2	Existing Channel Estimation Methods	29
3.2.1	Least-square Channel Estimation	29
3.2.2	DFT-based Channel Estimation	30
3.2.3	Chen's Method of Least-square Channel Estimation	31
3.2.4	Yeh's Algorithm of ICI-reduction Method	34
3.2.5	Simulation Results	38
<b>Chapter 4 The Proposed Data Detection and Channel Estimation Methods</b>		<b>44</b>
4.1	The Proposed Frequency-domain Successive Detection Methods	44
4.1.1	Algorithms of the Frequency-domain Successive Detection Methods	45
4.1.2	Complexity Analysis	48
4.2	The Proposed Channel Estimation Methods	55
4.2.1	Modification of Yeh's ICI-reduction Method	55
4.2.2	The Hybrid LS/ICI-reduction Channel Estimation Method	56
<b>Chapter 5 Simulation Results</b>		<b>58</b>
5.1	The Performances of the Proposed Frequency-domain Successive Detection methods	59
5.2	The Effect of Channel Estimation Error of the Proposed Frequency-domain Successive Detection Methods	65
5.3	The Performances of the Proposed Channel Estimation Methods	69
<b>Chapter 6 Conclusion</b>		<b>74</b>
<b>Bibliography</b>		<b>76</b>







# List of Tables

---

Table 3.1	Simulated OFDM system parameters	25
Table 3.2	Simulated OFDM system parameters	39
Table 3.3	ETSI Vehicular A channel environment	39
Table 4.1	Complexity statistics of the proposed and Choi's successive detection methods in the first detection layer	50
Table 4.2	Complexity statistics of the proposed and Choi's successive detection methods in the detection layer before the last one	50
Table 4.3	Complexity statistics of the proposed and Choi's successive detection methods in the first detection layer with $N = 64$ , and $q = 8, 4$	50
Table 4.4	Complexity statistics of the proposed and Choi's successive detection methods in the detection layer before the last one with $N = 64$ , and $q = 8, 4$	51
Table 4.5	Complexity statistics of the other mentioned methods	52
Table 4.6	Complexity ratio % of the detection methods $N = 64$ , $q = 8, 4$ and, $I = 3$	52

# List of Figures

---

Figure 2.1	Cyclic prefix of an OFDM symbol	7
Figure 2.2	Continuous-time OFDM baseband modulator	7
Figure 2.3	Spectrum of an OFDM symbol	8
Figure 2.4	Continuous-time OFDM baseband demodulator	9
Figure 2.5	Discrete-time OFDM system model	10
Figure 2.6	Illustrating the calculation of Doppler frequency	12
Figure 2.7	SIR for OFDM systems in time-varying channels	15
Figure 2.8	Normalized magnitude responses for different $f_{nd}$ 's	15
Figure 2.9	Channel impulse responses within an OFDM symbol for different $f_{nd}$ 's	16
Figure 3.1	Transformation of ICI matrix $\mathbf{G}$ to block diagonal $\mathbf{G}$ . $q = 2$	20
Figure 3.2	Choi's methods of successive detection	24
Figure 3.3	BER performances of the existing data detection methods in the two-ray equal power channel with $f_{nd} = 0.040$	26
Figure 3.4	BER performances of the existing data detection methods in the two-ray equal power channel with $f_{nd} = 0.083$	26
Figure 3.5	Regular pilot placement	30
Figure 3.6	Linear model between two consecutive OFDM symbols	36
Figure 3.7	Yeh's algorithm of ICI-reduction method	37
Figure 3.8	ANMSE performances of Chen's and Yeh's methods of channel estimation in the "Vehicular A" channel with $f_{nd} = 0.040$	40
Figure 3.9	ANMSE performances of Chen's and Yeh's methods of channel estimation in the "Vehicular A" channel with $f_{nd} = 0.083$	40
Figure 3.10	BER performances of Chen's and Yeh's methods of channel estimation	

---

	combined with data detection methods in the “Vehicular A” channel with $f_{nd} = 0.040$	41
Figure 3.11	BER performances of Chen’s and Yeh’s methods of channel estimation combined with data detection methods in the “Vehicular A” channel with $f_{nd} = 0.083$	41
Figure 4.1	The proposed frequency-domain successive detection methods	47
Figure 4.2	Modified linear model between two consecutive OFDM symbols	55
Figure 4.3	Procedure of the proposed channel estimation and data detection	57
Figure 5.1	BER performances of the data detection methods in the two-ray equal power channel with $f_{nd} = 0.040$	60
Figure 5.2	BER performances of the data detection methods in the two-ray equal power channel with $f_{nd} = 0.083$	60
Figure 5.3	BER performances of the data detection methods in the “Vehicular A” channel with $f_{nd} = 0.040$	61
Figure 5.4	BER performances of the data detection methods in the “Vehicular A” channel with $f_{nd} = 0.083$	61
Figure 5.5	BER performances of the proposed method in different detection layers in the “Vehicular A” channel with $f_{nd} = 0.083$	64
Figure 5.6	BER performances of the proposed method in different subcarriers in the “Vehicular A” channel with $f_{nd} = 0.083$	64
Figure 5.7	BER performances of the detection methods for $f_{nd} = 0.040$ , versus normalized mean square error $\eta$	67
Figure 5.8	BER performances of the detection methods for $f_{nd} = 0.083$ , versus normalized mean square error $\eta$	67

---

Figure 5.9	BER performances of the proposed detection methods for $f_{nd} = 0.040$ , versus normalized mean square error $\eta$	68
Figure 5.10	BER performances of the proposed detection methods for $f_{nd} = 0.083$ , versus normalized mean square error $\eta$	68
Figure 5.11	BER performances of the proposed detection methods for different normalized Doppler frequencies $f_{nd}$ 's, versus normalized mean square error $\eta$ in SNR = 35	69
Figure 5.12	ANMSE performances of the channel estimation methods in the “Vehicular A” channel with $f_{nd} = 0.040$	70
Figure 5.13	ANMSE performances of the channel estimation methods in the “Vehicular A” channel with $f_{nd} = 0.083$	70
Figure 5.14	BER performances of the channel estimation methods combined with data detection methods in the “Vehicular A” channel with $f_{nd} = 0.040$	71
Figure 5.15	BER performances of the channel estimation methods combined with data detection methods in the “Vehicular A” channel with $f_{nd} = 0.083$	71

# Chapter 1

## Introduction



In recent years, the demand for multimedia services increases rapidly, such as high quality video and audio data. Thus, the next generation communication systems are expected to provide high data rate transmissions. To satisfy these requirements, several transmission schemes must efficiently use transmission bandwidth. Multicarrier techniques are such transmission schemes widely adopted in commercial communication systems. When applied in a wireless environment, it is usually referred to as Orthogonal Frequency Division Multiplexing (OFDM). This modulation scheme has been adopted in many wireless transmission standards, such as wireless LAN (Local Area Network) IEEE 802.11a, wireless MAN (Metropolitan Area Network) IEEE 802.16, European Digital Audio Broadcasting (DAB) and Digital Video Broadcasting Terrestrial (DVB-T).

## 1.1 Background and Motivation

In OFDM systems, a high data-rate serial data stream is split into numerous low data-rate parallel data streams. They are modulated by several orthogonal subcarriers. For practical implementation, the oscillators generating subcarriers are replaced by inverse fast Fourier transform (IFFT) [1] [2] [3]. The spectrums of these modulated signals overlap each other over the frequency domain only except the frequency points where subcarriers allocate. This is why the transmission bandwidth is efficiently used in OFDM systems. The symbol duration is lengthened by the parallel transmission of the low data-rate data stream. This long symbol duration of the OFDM signal facilitate to mitigate the channel delay spread in wireless communication channels. By adding a cyclic prefix (CP) to the beginning of each OFDM symbol, the intersymbol interference (ISI), and intercarrier interference (ICI) caused by delay spread would be overcome. The corresponding channel response appears as a multiplication in the frequency domain. Therefore, a flat fading channel model can be assumed for each subchannel. A single tap equalizer is good enough for coherent detection. To perfectly combat the ICI, and ISI, the length of the CP must be longer than the maximum channel delay spread. However, the system throughput descends as the length of the CP increases.

Usually, it is assumed that the channel response is quasi-static within an OFDM symbol. With such assumption, the effect of the multipath channel equals a complex multiplication to the modulation at the subcarrier. This assumption is reasonable when the symbol duration is short or the transceivers are fixed. However, in some standards, such as DVB-T IEEE 802.16e, and IEEE 802.20, the symbol durations are very long and the systems are not only designed for the fixed users but also for mobile users. The channel response is not quasi-static within an OFDM symbol but time-varying.



Channel variations within an OFDM symbol destroy the orthogonality between sub-carriers and result in ICI. Conventional channel estimation techniques and 1-tap frequency-domain equalizer are subject to the ICI effect. The ICI effect degrades the system performance. The corresponding error floor becomes more severe as mobile speed, carrier frequency, or symbol duration increase, especially for higher-order modulation schemes [4] [5].

To mitigate the ICI due to channel variation, some detection and equalization methods, e.g., iterative ICI cancellation [6] [11] [27], least square (LS) detection [8] [18] [20], iterative LS detection [18], frequency-domain linear filter [21], and frequency-domain decision feed-back filter [22] [23] have been proposed. However, these approaches only treat ICI just as interference obstructing data detection and intend to suppress as much ICI as possible. Thus, the performances of these methods are bounded by the performance of the parallel detection in time-invariant channels. Choi et al. [7] showed a new idea that the time-varying nature of a channel can be exploited as a provider of time diversity and proposed a time-domain successive detection method. Therefore, their method can be applied to rapidly time-varying fading channels and outperform the other mentioned methods. However, the computational complexity of this method is too high to be realized.

Some channel estimation methods for time-varying fading channels, e.g., iterative LS estimation [24], frequency-domain pilot-symbol-aided MMSE estimation [7] [21], frequency-domain pilot-symbol-aided estimation [25], and time-domain pilot-symbol-aided estimation [8] [22] also have been proposed. However, time-domain low-pass filter applied in [24] can not suppress ICI perfectly when channel variation increases. MMSE estimation in [7] needs pilot symbols for long time duration. Thus, the approach suffers long system latency. Besides, MMSE estimation in [7] [21] requires the characteristics of the fading channels so that it is hard to be realized. The

approach in [25] can only be used in flat fading channels. The structures of the time-domain pilot symbols used in [8] [22] are different from that of the frequency-domain pilot patterns applied in commercial systems. Besides, the approaches in [8] [22] can only be used in slowly time-varying channels. In [6] [18], the authors have proposed a mathematical model used in the channel estimation assuming linear channel variation.

Based on the existing channel estimation methods [6] [18] and the data detection methods [7] [8], several modified methods to improve the system performances or to reduce the system computational complexities are proposed in this thesis. The proposed data detection methods exploit the time diversity involved in the nature of the time-varying channels, which is introduced in [7]. Thus, the proposed methods outperform the conventional methods [6] [8] [11] [20] [21] [22] [23] [27]. For implementation, the proposed methods are modified to have acceptable complexities by utilizing the technique introduced in [8]. The proposed channel estimation method is based on appropriate mathematical models modified from [6] [11] [18]. As a result, the estimated parameters can be reduced. Therefore, channel estimation under fast fading conditions becomes feasible and trackable.

## 1.2 Organization of the Thesis

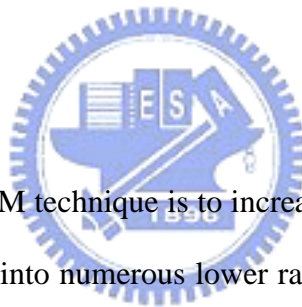
This thesis is organized as follows. In Chapter 2, the fundamentals of OFDM systems and the characteristics of wireless multipath Rayleigh fading channels are described. Then, ICI effect of OFDM systems in time-varying channels is analysis. In Chapter 3, five existing data detection methods, single tap equalization, least square (LS) detection, Jeon's method of LS detection, ICI cancellation, and Choi's method of successive detection are introduced. Performances of these data detection methods are

evaluated. Then, two conventional channel estimation methods, LS channel estimation and discrete-time Fourier transform (DFT)-based channel estimation, are presented. Two channel estimation methods for OFDM systems in time-varying channels are introduced. In the end of this chapter, performances of these channel estimation methods are evaluated. In Chapter 4, the proposed data detection methods are introduced. Also, computational complexities of the proposed data detection methods are evaluated. Then, the proposed channel estimation methods are introduced. In Chapter 5, performances of the proposed data detection methods and the channel estimation methods are evaluated. Also, the effect of channel estimation error is discussed. In Chapter 6, conclusion is given.



## Chapter 2

# Fundamentals of OFDM Systems



The basic concept of OFDM technique is to increase the symbol duration by splitting the high-rate data stream into numerous lower rate streams and equally to divide the available transmission spectrum into several narrowband subchannels. These low rate streams are transmitted simultaneously over these subchannels. The overlapping and orthogonal transmission spectrums of modulated signals are designed for high spectral efficiency. Due to the property of narrowband, each modulated signal transmitted in the subchannel almost experiences flat fading. Therefore, the channel equalization is simplified as a single-tap equalization. On the other hand, the lengthened OFDM symbol appended with a preceding CP helps mitigate the ICI and ISI effects. A CP is the extension of an OFDM symbol that equals the tail part of the symbol, which is shown in Figure 2.1, and must be larger than the maximum channel delay spread to avoid ISI. Thus, the signals and their own delayed-version signals resulting from the multipath channel are still whole periodic waves within the DFT in-

terval. The orthogonality between subcarriers can be maintained after the modulated signals pass through the multipath channel, i.e. no ICI.

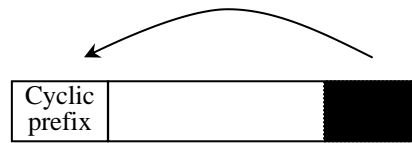
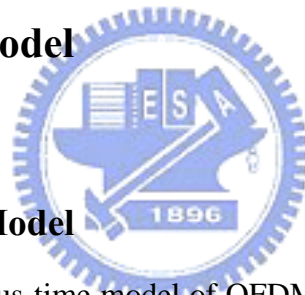


**Figure 2.1** Cyclic prefix of an OFDM symbol [11]

However, when symbol durations are very long or users have mobility, the channel response is not quasi-static within an OFDM symbol but time-varying. Channel variations within an OFDM symbol destroy the orthogonality between subcarriers and result in ICI. This phenomenon will be depicted in Section 2.3.

## 2.1 OFDM System Model



### 2.1.1 Continuous-time Model

In this section, a continuous-time model of OFDM system is investigated. A typical continuous-time OFDM baseband modulator is shown in Figure 2.2. The input data stream is split into  $N$  parallel streams which are modulated by  $N$  different subcarriers and then transmitted simultaneously.

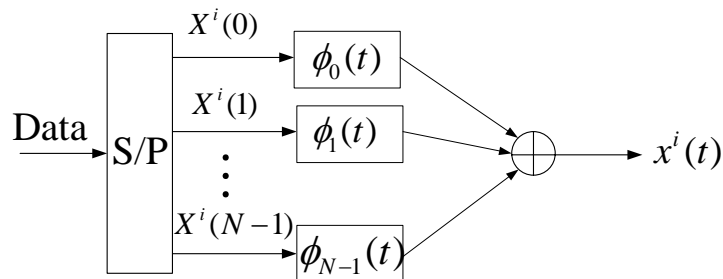


**Figure 2.2** Continuous-time OFDM baseband modulator

The  $k$ -th modulating subcarrier is

$$\phi_k(t) = \begin{cases} e^{\frac{j2\pi k(t-T_g)}{T}}, & 0 \leq t \leq T_s \\ 0, & \textit{otherwise} \end{cases} \quad (2.1)$$

where  $T$  is the symbol duration exclusive of CP,  $T_g$  is the length of CP and  $T_s$  is the total symbol duration, i.e.  $T_s = T + T_g$ .  $X^i(k)$  is defined as the transmitted data which is a complex number from a set of signal constellation points at the  $k$ -th subcarrier for the  $i$ -th symbol. The modulated baseband signal of the  $i$ -th OFDM symbol is

$$x^i(t) = \sum_{k=0}^{N-1} X^i(k)\phi_k(t - iT_s) \quad (2.2)$$

When an infinite sequence of OFDM symbols is transmitted, the output of the transmitter can be represented as

$$x(t) = \sum_{i=-\infty}^{\infty} x^i(t) = \sum_{i=-\infty}^{\infty} \sum_{k=0}^{N-1} X^i(k)\phi_k(t - iT_s) \quad (2.3)$$

The overlapping and orthogonal transmission spectrums of the modulated signals are shown in Figure 2.3. Because of the sinc shape of the spectrums of these modulated signals, the spectrums of them overlap with each other over the frequency domain only except the frequency points where subcarriers allocate. The subcarrier spacing between any two neighbor subcarriers is  $\frac{1}{T}$ . Thus, OFDM systems have high bandwidth efficiency.

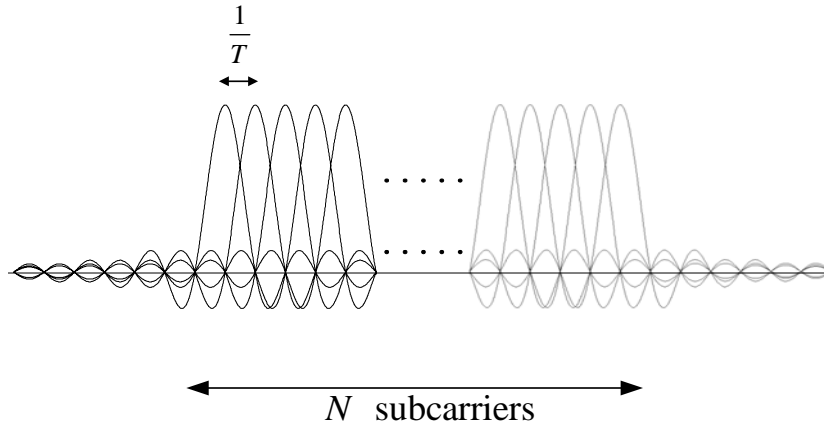


**Figure 2.3** Spectrum of an OFDM symbol [11]

The received signal  $y(t)$  can be expressed as

$$y(t) = \int_{-\infty}^{\infty} h(t, \tau)x(t - \tau)d\tau + w(t) \quad (2.4)$$

where time-variant channel impulse response at time  $t$  is  $h(t, \tau)$ , and  $w(t)$  is an additive white complex Gaussian noise.

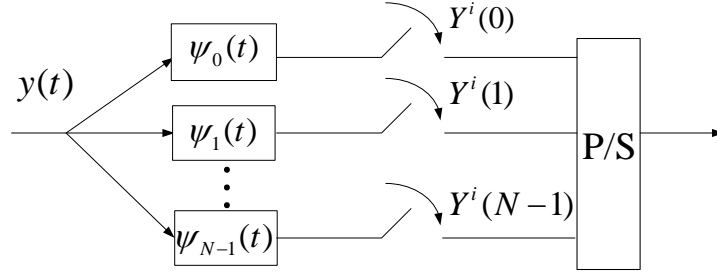


**Figure 2.4** Continuous-time OFDM baseband demodulator

An typical continuous-time OFDM baseband demodulator is drawn in Figure 2.4.

$\psi_k(t)$  is the matched filter for the  $k$ -th subcarrier.

$$\psi_k(t) = \begin{cases} \frac{1}{T} e^{j2\pi kt/T}, & 0 \leq t \leq T_s \\ 0, & \text{otherwise} \end{cases} \quad (2.5)$$

$Y^i(k)$  is the demodulated signal at the  $k$ -th subcarrier for the  $i$ -th symbol.

### 2.1.2 Discrete-time Model

In [3], Weinstein suggested that the modulators in the transmitter and the matched filters in the receiver for the OFDM systems can be implemented by IDFT and DFT, respectively. Also, the fast DFT/IDFT algorithm, FFT/IFFT, can be applied to the OFDM systems. Figure 2.5 shows the discrete-time OFDM system model.

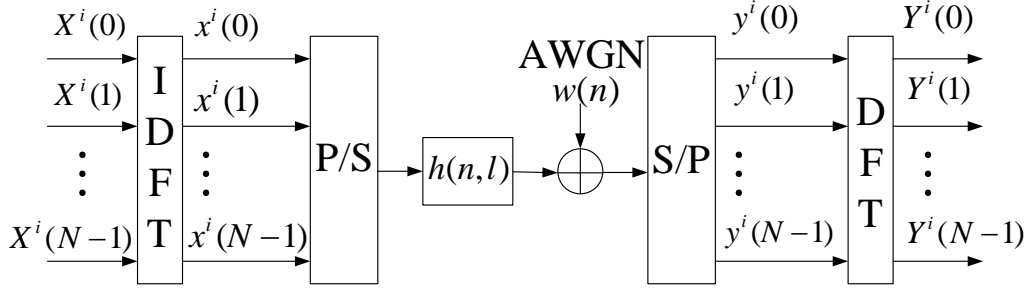


**Figure 2.5** Discrete-time OFDM system model

Without loss of generality, the symbol index  $i$  is dropped in the following discussion.

The modulated signal can be written as

$$x(n) = \sum_{k=0}^{N-1} X(k) e^{j2\pi kn/N} \quad (2.6)$$

where  $X(k)$  is the transmitted data at the  $k$ -th subcarrier, and  $0 \leq n \leq N-1$ . Then, the modulated signal appended with a preceding CP is delivered over the air and experiences a time-varying and multipath fading channel. Therefore, the received signal can be represented as

$$y(n) = \sum_{l=0}^{L-1} h(n, l) x(n-l)_N + w(n) \quad (2.7)$$

where  $h(n, l)$  is the  $l$ -th channel path at time instant  $t = n \times t_s$ ,  $t_s = \frac{T}{N}$  is sampling period,  $L$  is the number of channel taps,  $(\cdot)_N$  represents a cyclic shift in the base of  $N$ , and  $w(n)$  is sampled additive white complex Gaussian noise with variance  $\sigma^2$ .

The received signal after DFT at the  $k$ -th subcarrier is

$$Y(k) = \sum_{n=0}^{N-1} y(n) e^{-j2\pi kn/N} \quad (2.8)$$

## 2.2 Channel Characteristics in Wireless Communication Environments

The transmitted signal propagates along several different paths through the wireless channel and arrives at the receiver. Such environment is referred to as a multipath



channel. These paths arise from scattering, reflection, and diffraction of the radiated energy by objects in the environment or refraction in the medium. These duplicated signals add together at the receiver. Thus, the corresponding received signal is distorted. The amplitude of the received signal fluctuates with location and time. This phenomenon is referred to as fading.

The impulse response of the fading channel can be expressed as

$$h(t, \tau) = \sum_{l=0}^{L-1} \alpha_l(t) \delta(\tau - \tau_l) \quad (2.9)$$

where  $L$  is the number of resolvable channel paths, and  $\alpha_l(t)$  and  $\tau_l$  are the path gain and the path delay time of the  $l$ -th resolvable channel path, respectively. The path gain  $\alpha_l(t)$  is modeled as [9] [10] for all  $l$ .

$$\alpha_l(t) = \sum_{n=1}^M C_{n,l} e^{j(2\pi f_d t \cos \gamma_{n,l} + \phi_{n,l})} \quad (2.10)$$

where  $M$  is the number of the unresolvable paths,  $C_{n,l}$ ,  $\gamma_{n,l}$ , and  $\phi_{n,l}$  are respectively the random path gain, the angle of the incoming wave, and the initial phase associated with the  $n$ -th unresolvable of the  $l$ -th resolvable path, and  $f_d$  is the maximum Doppler frequency.

The central limited theorem justifies that  $\alpha_l(t)$  can be approximated as complex Gaussian random process for large  $M$  [10].  $\gamma_{n,l}$ , and  $\phi_{n,l}$  are assumed to be mutually independent and to be uniformly distributed over  $[-\pi, \pi)$  for all  $n$  and  $l$ . Further, if path delay time of the resolvable path,  $\tau_l$ , is sample-spaced, i.e.  $\tau_l = l \times t_s$  and  $l$  is an integer, for all  $l$ . The impulse response of the fading channel can be simplified as

$$h(n, l) = \alpha_l(nt_s) \quad (2.11)$$

for  $l = 0, \dots, L-1$ .

To specify the relationship between the variation of the fading channel and the

motion of the receiver in (2.10), consider the situation illustrated in Figure 2.6.

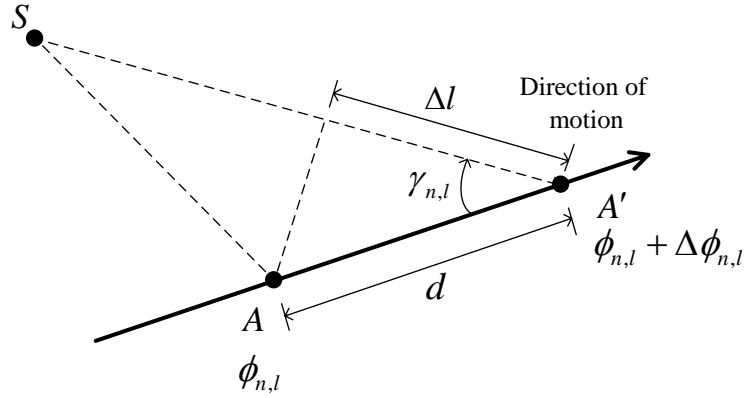


**Figure 2.6** Illustrating the calculation of Doppler frequency

It is assumed that the transmitted signal propagating along the  $l$ -th path is modeled as the source  $S$  which is far away from the mobile station  $A$ . The mobile station  $A$  moves from the point  $A$  to the point  $A'$  in the time duration from  $0$  to  $t$ . Thus, the change in the phase angle of the received signal between the point  $A$  and the point  $A'$  is given by

$$\begin{aligned}
 \Delta\phi_{n,l} &= \frac{2\pi}{\lambda} \Delta l \\
 &= 2\pi \frac{f_c}{C} d \cos \gamma_{n,l} \\
 &= 2\pi \frac{f_c v}{C} t \cos \gamma_{n,l} \\
 &= 2\pi f_d t \cos \gamma_{n,l}
 \end{aligned} \tag{2.12}$$

where  $\lambda$ ,  $f_c$ ,  $C$ , and  $v$  are the radio wavelength, radio center frequency, velocity of light, and velocity of the mobile station, respectively, and  $f_d \triangleq \frac{f_c v}{C}$  is the maximum Doppler frequency occurring at  $\gamma_{n,l} = 0$ . In conclusion, the variation of the fading channel is proportional to the ratio center frequency and velocity of the mobile receiver.

## 2.3 Analysis of Intercarrier Interference

According to the system model depicted in Section 2.1.2 and the channel model described in Section 2.2, the received signal after DFT at the  $k$ -th subcarrier is expressed as

$$Y(k) = \sum_{n=0}^{N-1} y(n) e^{-\frac{j2\pi kn}{N}} \quad (2.8)$$

Substitute equations (2.6) and (2.7) into (2.8)

$$Y(k) = G(k, k)X(k) + \underbrace{\sum_{m=0, m \neq k}^{N-1} G(k, m)X(m)}_{ICI} + W(k) \quad (2.13)$$

where  $G(k, m) = \frac{1}{N} \sum_{r=0}^{N-1} \sum_{l=0}^{L-1} h(r, l) e^{\frac{j2\pi r(m-k)}{N}} e^{-\frac{j2\pi lm}{N}}$ ,  $W(k) = \sum_{n=0}^{N-1} w(n) e^{-\frac{j2\pi kn}{N}}$ ,

$0 \leq m \leq N-1$ , and  $0 \leq k \leq N-1$ . Since the second term on the right hand side of equation (2.13) is not zero, the desired signal suffers ICI when the channel is time-varying. On the contrary, ICI terms will vanish if  $f_d$  in (2.10) equals zero, i.e. time-invariant channel. For further ICI analysis when  $f_d \neq 0$ , let's first define the time average of channel impulse response,  $h(n, l)$ , as

$$h_{ave}(l) = \frac{1}{N} \sum_{n=0}^{N-1} h(n, l) \quad (2.14)$$

and the variation  $\Delta h(n, l)$  of  $h(n, l)$  as

$$\Delta h(n, l) = h(n, l) - h_{ave}(l) \quad (2.15)$$

Therefore,

$$G(k, k) = \sum_{l=0}^{L-1} h_{ave}(l) e^{-\frac{j2\pi lk}{N}} \quad (2.16)$$

and

$$G(k, m) = \frac{1}{N} \sum_{r=0}^{N-1} \sum_{l=0}^{L-1} \Delta h(r, l) e^{\frac{j2\pi r(m-k)}{N}} e^{-\frac{j2\pi lm}{N}}, \quad m \neq k \quad (2.17)$$

If the channel impulse response is time-invariant,  $\Delta h(n, l)$  equals zero and  $G(k, m) = 0$ ,  $m \neq k$ .

The received signal after DFT can be rewritten as the following matrix form

$$\mathbf{Y} = \frac{1}{N} \mathbf{Q} \mathbf{H} \mathbf{Q}^H \mathbf{X} + \mathbf{W} \quad (2.18)$$

where  $\mathbf{Y} = [Y(0), \dots, Y(N-1)]^T$ ,  $\mathbf{X} = [X(0), \dots, X(N-1)]^T$ ,  $\mathbf{W} = [W(0), \dots, W(N-1)]^T$ ,  $\mathbf{H}(n, m) = h(n, (n-m)_N)$ , and  $\mathbf{Q}$  is the  $N$ -point DFT matrix with its elements  $Q(n, m) = e^{-j2\pi mn/N}$ . For convenience,  $\mathbf{G}$  is defined as  $\mathbf{G} \triangleq \frac{1}{N} \mathbf{Q} \mathbf{H} \mathbf{Q}^H$ . Thus, the received signal after DFT can be written as

$$\mathbf{Y} = \mathbf{G} \mathbf{X} + \mathbf{W} \quad (2.19)$$

The effects of ICI have been analyzed in some papers. Li et al. [4] stated that in order to achieve signal to intercarrier interference ratio (SIR)  $> 20\text{dB}$ , the OFDM symbol duration must be less than 8% of the channel coherence time ( $T_{\text{coherence}} = 1/f_d$ ) when a Wide-Sense Stationary and Uncorrelated Scattering (WSSUS) channel is considered. This effect is shown in Figure 2.7. In [8], Jeon et al. concluded that when the multipath fading channel is slowly time-varying (Normalized Doppler frequency  $< 0.1$ ), ICI terms which do not significantly affect  $Y(k)$  can be ignored and time variation of the channel impulse response can be approximated by a straight line. These ideas are illustrated in Figure 2.8 and Figure 2.9, respectively. The normalized Doppler frequency,  $f_{nd}$ , is defined as

$$f_{nd} \triangleq f_d T_{ob} \quad (2.20)$$

where  $T_{ob}$  is the observation duration. It is used to quantify the variation of the fading channel within the observation duration. Thus, when considering the variation of the fading channel within an OFDM symbol, the observation duration is set to the symbol duration. In this thesis, the investigation focuses on the effect of ICI within an OFDM symbol, i.e.  $T_{ob} = T$ . In conclusion, OFDM systems suffer more ICI as normalized Doppler frequency increases.

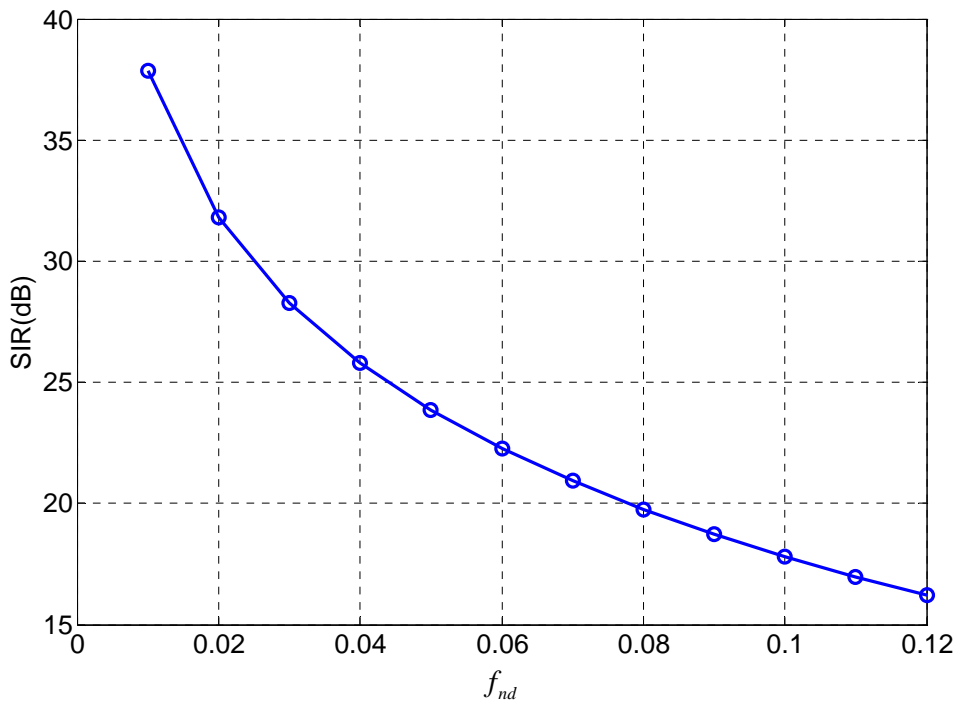


Figure 2.7 SIR for OFDM systems in time-varying channels [4]

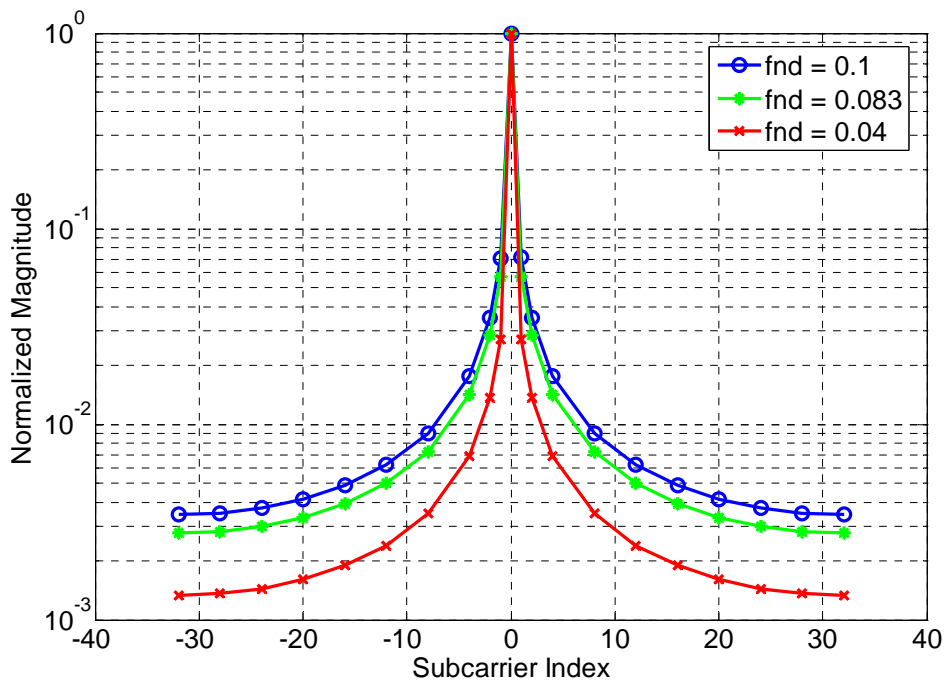
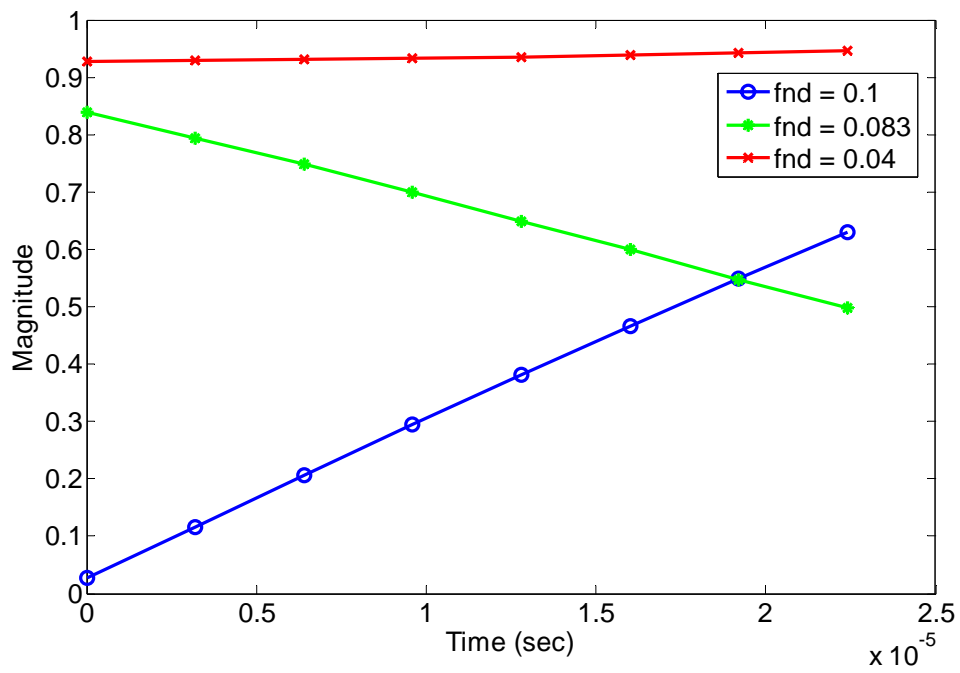


Figure 2.8 Normalized magnitude responses for different  $f_{nd}$ 's [8]



**Figure 2.9** Channel impulse responses within an OFDM symbol for different  $f_{nd}$  's



## Chapter 3

# Investigation of Existing Data Detection and Channel Estimation Methods



A signal propagating through wireless channels will be distorted by its own duplications. The received signal would have a random phase rotation, and the magnitude of the received signal would be attenuated. This phenomenon has been depicted in Section 2.2. In order to coherently detect the transmitted data, the random phase rotation and the magnitude attenuation must be obtained and compensated before demapping the symbols according to the modulation constellation. In this chapter, existing common data detection methods for compensation of the received signal are first introduced. Then, several channel estimation methods for obtaining channel state information are described. These methods are all evaluated by computer simulations. The advantages and the disadvantages of these methods are indicated according to the simulation results.

### 3.1 Existing Data Detection Methods

Several existing data detection methods are introduced in this section. The simulation results show that performances of the first four methods are not good enough in the assumed common channel environments. Only, Choi's method of successive detection performs well in the assumed environments. In the following discussion, the system model introduced in Section 2.3 is considered.

#### 3.1.1 Single-tap Equalization

The impulse response of a slow-fading channel is generally quasi-static within an OFDM symbol. Therefore, there is approximately no ICI between subcarriers. According to (2.13), the compensation for each subcarrier is equivalent to single-tap frequency-domain equalization.

$$Z(k) = \frac{Y(k)}{G(k,k)} \quad (3.1)$$

Then, the equalized signal  $Z(k)$  is passed through a signal demapper. The demodulated data are obtained. This method is simple and widely used in indoor OFDM systems. However, in time-varying fading channels, single-tap equalization will be distorted by ICI. As such, there would be an irreducible error floor.

#### 3.1.2 Least-square Detection (Decorrelating Detection)

Increasing the taps of an equalization process is a straightforward method to suppress the ICI introduced by time-varying fading channels. Given by the linear model (2.18) and basic linear algebra theory, the least-square (LS) detection is expressed by

$$\mathbf{Z} = \mathbf{G}^+ \mathbf{Y} \quad (3.2)$$

where  $\mathbf{G}^+ = (\mathbf{G}^H \mathbf{G})^{-1} \mathbf{G}^H$  is the pseudo inversion of  $\mathbf{G}$ . LS detection can suppress ICI perfectly. However, noise enhancement would be induced when the correlations



of the elements in  $\mathbf{G}$  are high. Besides, the computational complexity of the LS detection is proportional to  $O(N^3)$  [16] when  $\mathbf{G}$  is a square matrix with dimension of  $N$ . Thus, this detection method is hard to be implemented for the OFDM systems with numerous subcarriers, such as DVB-T and IEEE 802.16e.

### 3.1.3 Jeon's Method of Least-square Detection

The LS detection described in the previous section is widely used for interference suppression. However, its computational complexity is proportional to  $O(N^3)$ .  $N$  is the number of mixed signals. For OFDM systems,  $N$  is the number of subcarriers due to the loss of the orthogonality between subcarriers in time-varying fading channels.

Jeon et al. [8] proposed a method for computational complexity reduction of LS detection. After ICI analysis, they concluded that when the multipath fading channel is slowly time-varying (Normalized Doppler frequency  $f_{nd} < 0.1$ ), most power of channel frequency response concentrates on the neighborhood of the subcarriers. Thus, those ICI terms which do not significantly affect  $Y(k)$  can be ignored, i.e.

$$G(m, k) = 0, \quad |m - k| > q/2 \quad (3.3)$$

where  $q$  denotes the number of dominant ICI terms. Figure 2.8 depicts this property, obviously. In physical meaning, the diagonal terms of  $\mathbf{G}$  can be viewed as the D.C. components of the time variation of the channel response, and the neighbor terms of them are the corresponding lowpass components according to equations (2.14)-(2.17). By Jeon's conclusion, the power of the channel response concentrates on the lowpass band in Doppler spectrum domain. Thus, high frequency components of channel variation could be ignored when the fading channel is slowly time-varying.

Consequently, the matrix  $\mathbf{G}$  becomes sparse and can be transformed as a block diagonal matrix  $\mathcal{G} = \text{diag}([\mathbf{G}_{blk,0}, \mathbf{G}_{blk,1}, \dots, \mathbf{G}_{blk,N-1}])$  as shown in Figure 3.1. Note that

there are some revisions compared to Jeon's method.

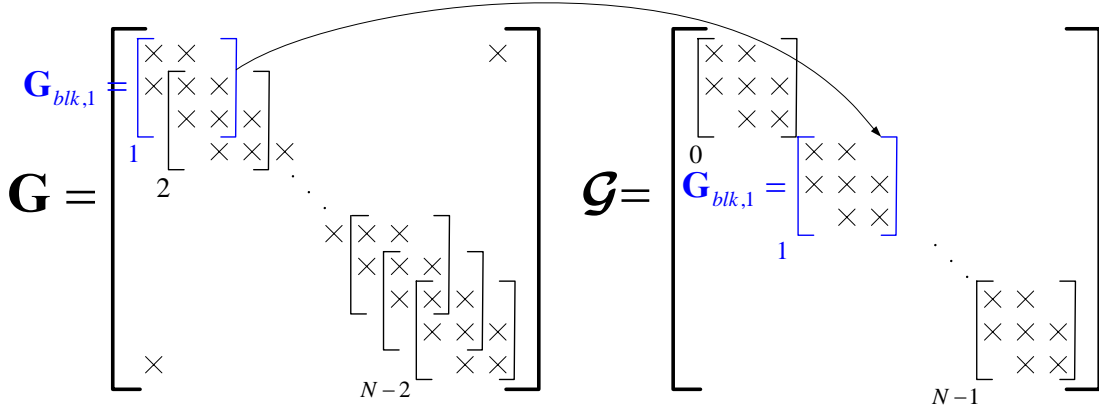


**Figure 3.1** Transformation of ICI matrix  $\mathbf{G}$  to block diagonal  $\mathbf{G}$ .  $q = 2$  [8]

The system model given in (2.19) is transformed as overlapped block-diagonal

$$\mathbf{y} = \mathbf{G}\mathbf{x} + \mathbf{w} \quad (3.4)$$

where

$$\begin{aligned} \mathbf{y} &= [\mathbf{Y}_{blk,0} \mathbf{Y}_{blk,1} \cdots \mathbf{Y}_{blk,N-1}]^T \\ \mathbf{x} &= [\mathbf{X}_{blk,0} \mathbf{X}_{blk,1} \cdots \mathbf{X}_{blk,N-1}]^T \\ \mathbf{w} &= [\mathbf{W}_{blk,0} \mathbf{W}_{blk,1} \cdots \mathbf{W}_{blk,N-1}]^T \\ \mathbf{X}_{blk,k} &= [X(k - q/2)_N \cdots X(k) \cdots X(k + q/2)_N]^T \\ \mathbf{Y}_{blk,k} &= [Y(k - q/2)_N \cdots Y(k) \cdots Y(k + q/2)_N]^T \\ \mathbf{W}_{blk,k} &= [W(k - q/2)_N \cdots W(k) \cdots W(k + q/2)_N]^T \end{aligned} \quad (3.5)$$

The D.C. components of channel variation and the corresponding dominated ICI terms between subcarriers are separated into a number of sub blocks which do not interfere with each other. Therefore, LS detection of the original system is modified as LS detections of the blocked systems

$$\mathbf{z}_k = \mathbf{G}_{blk,k}^+ \mathbf{Y}_{blk,k} \quad (3.6)$$

where  $k = 0, 1, \dots, N-1$ . The middle element of the equalized vector  $\mathbf{z}_k$  is an approximation to the  $k$ -th element of the vector  $\mathbf{z}$  in (3.2). Therefore, instead of computing the matrix inversion of the entire  $\mathbf{G}$ ,  $N$  matrix inversions of smaller  $\mathbf{G}_{blk,k}$ 's

are needed in the simplified technique. The computational complexity of LS detection is reduced from  $O(N^3)$  to  $O(N(q+1)^3)$ . Usually,  $q \ll N$ . Thus, the reduction is large.

### 3.1.4 Intercarrier Interference Cancellation

In order to avoid the noise enhancement problem and further reduce the computational complexity, the intercarrier interference (ICI) cancellation methods have been proposed [6] [11]. It is a kind of nonlinear detection methods with the decision-directed technique. The demodulated symbols are reconstructed and fed back to cancel ICI. The significant idea is to exploit the discreteness property of the modulated symbols in digital communication systems. Based on the discreteness property, most ICI would be cancelled after several iterations when the initial demodulated symbols are with acceptable correctness. Therefore, the demodulated symbols become increasingly correct during the iterative detection procedure. The ICI cancellation method proceeds as follows:

**Step 1:** Ignoring the ICI effect, the received signal  $\mathbf{Y}$  is divided by the single tap equalization, i.e.  $Z(k) = \frac{Y(k)}{G(k,k)}$ . Then, the equalized signal  $\mathbf{Z}$  is passed through a hard decision device or a demapper. The demodulated symbol,  $\hat{\mathbf{X}}$ , is obtained. Since the result is affected by ICI, some demodulated data may be erroneous.

**Step 2:** Performing ICI cancellation on the received signal  $\mathbf{Y}$ , i.e.  $\mathbf{Y}_I = \mathbf{Y} - \mathbf{G}_{ici} \hat{\mathbf{X}}_{I-1}$ . Thus, the ICI effect in the received signal  $\mathbf{Y}_I$  is reduced.  $I$  represents the iteration number.  $\mathbf{G}_{ici}$  denotes the channel response obtained from  $\mathbf{G}$  only with the ICI elements.

**Step 3:** The signal  $\mathbf{Y}_I$  after ICI cancellation is divided by the single tap equaliza-

tion, i.e.  $Z_I(k) = \frac{Y_I(k)}{G(k,k)}$ . Then, the equalized signal  $Z_I$  is passed through a hard

decision device or a demapper. The demodulated symbol,  $\hat{X}_I$ , is obtained.

**Step 4:** End if  $I = I_{\max}$ , otherwise repeat Steps 2 and 3 with  $I = I + 1$ .

The complexity of the ICI cancellation is proportional to  $O(N^2)$  due to ICI cancellation procedure in Step 2. For further complexity reduction, Chen et al. [6] suggested that ICI cancellation procedure can be perform in the time domain. However, it requires two more FFT operations.

### 3.1.5 Choi's Method of Successive Detection

All the mentioned data detection methods treat the ICI induced by time-varying fading channels just as the interference obstructing data detection. Choi et al. [7] suggested that the time-varying nature of the channel can be exploited as a provider of time diversity. Since the channel response is time-selective, the signal samples received at different time instants have low correlation and provide the diversity. In order to utilize the time diversity provided by time-selective channels, the successive layered detection from [15] performs in the time domain instead of detecting all the data in the frequency domain simultaneously. The data demodulated in the later layers gain more time diversity.

Recall the system model described in Section 2.1.2, the received signal is represented as

$$y(n) = \sum_{l=0}^{L-1} h(n,l)x(n-l)_N + w(n) \quad (2.7)$$

Substitute equation (2.6) into (2.7), the received signal can be represented as

$$y(n) = \frac{1}{N} \sum_{k=0}^{N-1} X(k)V(k,n)e^{\frac{j2\pi kn}{N}} + w(n) \quad (3.7)$$

where  $V(k,n) = \sum_{l=0}^{L-1} h(n,l)e^{-\frac{j2\pi lk}{N}}$ . Further, the received signal can be rewritten as the

matrix form

$$\mathbf{y} = \mathbf{V}\mathbf{X} + \mathbf{w} \quad (3.8)$$

where  $\mathbf{y} = [y(0), \dots, y(N-1)]^T$ ,  $\mathbf{w} = [w(0), \dots, w(N-1)]^T$ , and  $\mathbf{V} = \frac{1}{N} \mathbf{H}\mathbf{Q}^H$ .

The Choi's method of successive layered detection proceeds in Figure 3.2. In the method,  $\mathbf{u}_k$  and  $\mathbf{v}_k$  are the  $k$ -th column vectors of the matrices  $\mathbf{U}$  and  $\mathbf{V}$ , respectively.  $\sigma^2$  is the variance of the additive white complex Gaussian noise. The symbol "slice( )" is the hard decision device, i.e. demapper.

In each detection layer, it is necessary to recalculate the matrix inversion in Step P-5. Unfortunately, the number of detection layers and the dimension of the matrix  $\mathbf{V}$  increase as the number of subcarriers,  $N$ , gets larger. According to Section 3.1.2, the computational complexity of LS detection is proportional to  $O(N^3)$ . Thus, the computational complexity of this detection method is unacceptable for realization when  $N$  is too large.



Least Square (LS) Version
---------------------------

$$j = 1$$

$$\mathbf{U}^H = \mathbf{V}^+ \quad (P-1)$$

$$i_1 = \arg \min_k \|\mathbf{u}_k\|^2 \quad (P-2)$$

Loop

$$z(i_j) = \mathbf{u}_{i_j}^H \mathbf{y} \quad (P-3)$$

$$\hat{X}(i_j) = \text{slice}(z(i_j))$$

$$\mathbf{y} = \mathbf{y} - \mathbf{v}_{i_j} \hat{X}(i_j) \quad (P-4)$$

$$\mathbf{V} = [\mathbf{v}_0, \dots, \mathbf{v}_{i_j-1}, \mathbf{0}, \mathbf{v}_{i_{j+1}}, \dots, \mathbf{v}_{N-1}]$$

$$\mathbf{U}^H = \mathbf{V}^+ \quad (P-5)$$

$$i_{j+1} = \arg \min_{k \notin \{i_1, \dots, i_j\}} \|\mathbf{u}_k\|^2 \quad (P-6)$$

$$j = j + 1$$

Minimum Mean Square Error (MMSE) Version
--

$$j = 1$$

$$\mathbf{U}^H = (\mathbf{V}^H \mathbf{V} + \sigma^2 \mathbf{I})^{-1} \mathbf{V}^H \quad (P-1)$$

$$i_1 = \arg \max_k \frac{|\langle \mathbf{u}_k, \mathbf{v}_k \rangle|^2}{\sum_{m, m \neq k} |\langle \mathbf{u}_k, \mathbf{v}_m \rangle|^2 + \sigma^2 \|\mathbf{u}_k\|^2} \quad (P-2)$$

Loop

$$z(i_j) = \mathbf{u}_{i_j}^H \mathbf{y} \quad (P-3)$$

$$\hat{X}(i_j) = \text{slice}(z(i_j))$$

$$\mathbf{y} = \mathbf{y} - \mathbf{v}_{i_j} \hat{X}(i_j) \quad (P-4)$$

$$\mathbf{V} = [\mathbf{v}_0, \dots, \mathbf{v}_{i_j-1}, \mathbf{0}, \mathbf{v}_{i_{j+1}}, \dots, \mathbf{v}_{N-1}]$$

$$\mathbf{U}^H = (\mathbf{V}^H \mathbf{V} + \sigma^2 \mathbf{I})^{-1} \mathbf{V}^H \quad (P-5)$$

$$i_{j+1} = \arg \max_{k \notin \{i_1, \dots, i_j\}} \frac{|\langle \mathbf{u}_k, \mathbf{v}_k \rangle|^2}{\sum_{m, m \neq k, m \notin \{i_1, \dots, i_j\}} |\langle \mathbf{u}_k, \mathbf{v}_m \rangle|^2 + \sigma^2 \|\mathbf{u}_k\|^2} \quad (P-6)$$

$$j = j + 1$$

**Figure 3.2** Choi's methods of successive detection

### 3.1.6 Simulation Results

Several existing data detection methods are introduced above. In this section, performances of these methods are evaluated by computer simulations. For next-generation communication systems, wireless terminals are expected to operate at high radio frequencies, at high levels of mobility, and with high bandwidth efficiency. Thus, the targeted radio frequency, and the signal bandwidth specified in IEEE 802.20 TDD mode [12] are considered. The simulated OFDM system parameters are listed in Table 3.1. The typical two-ray equal power channel model is considered here. For the simulations, the channel power is normalized to 1. The multipath Rayleigh fading channels in the simulations are generated by the modified Jakes' model [9] [10]. It is assumed that the perfect channel information is known at the receiver and that synchronization is perfect.

**Table 3.1** Simulated OFDM system parameters

Operating frequency	3.5GHz
Signal bandwidth	2.5MHz
FFT length	64
Number of pilot subcarriers	16
Number of data subcarriers	48
Symbol duration	25.6us
Subcarrier spacing	39.1kHz
Modulation	QPSK
Channel coding	No
Power delay profile	Two-ray equal power
Normalized Doppler frequency	0.083 and 0.040

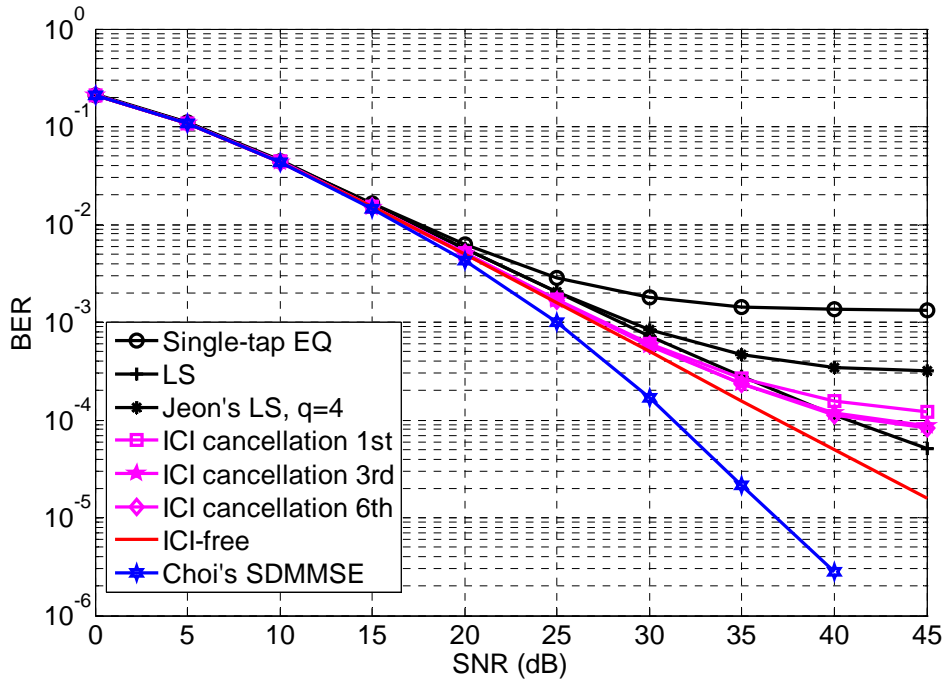


**Figure 3.3** BER performances of the existing data detection methods in the two-ray equal power channel with  $f_{nd} = 0.040$

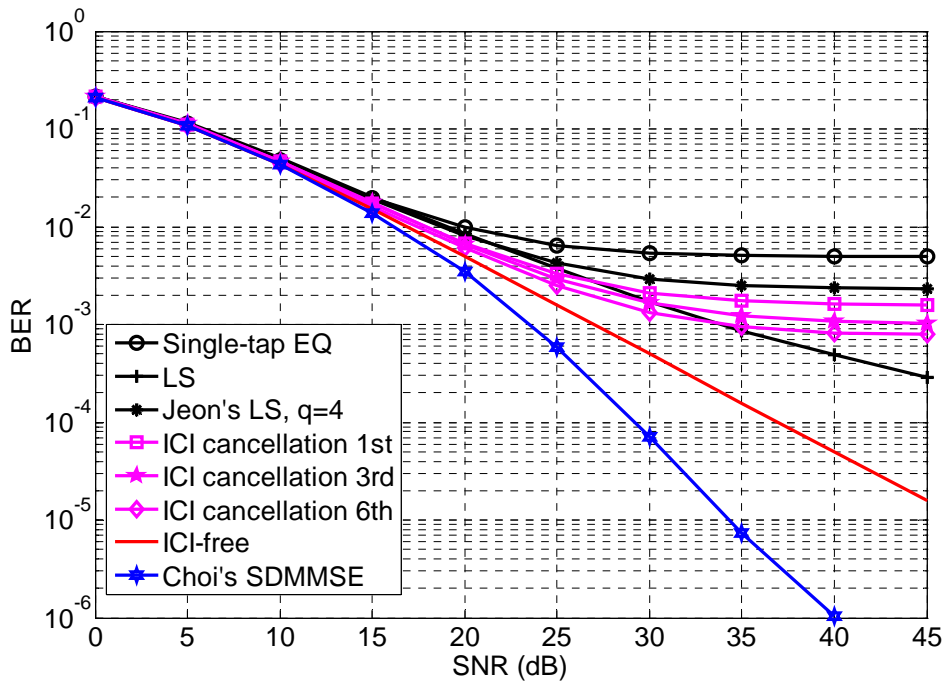


**Figure 3.4** BER performances of the existing data detection methods in the two-ray equal power channel with  $f_{nd} = 0.083$



The BER performances of the mentioned methods in the two-ray equal power channel with different  $f_{nd}$ 's are shown in Figure 3.3 and Figure 3.4, respectively. The term “ICI-free” indicates the theoretical BER performance of the coherent detection in the time-invariant flat Rayleigh fading channel for the reference of the ICI-free case. It is known that the BER performances of the first four mentioned detection methods are bounded by the ICI-free curve in the figure. The terms “Single tap EQ” and “LS” indicate the single-tap equalization and LS detection, respectively. The ordinal numbers appended to the term “ICI cancellation” indicate the numbers of the iterations of the ICI cancellation method. Jeon’s method of LS detection [8] is denoted as Jeon’s LS. The terms “q=number” appended to “Jeon’s LS” indicate the number of the dominant ICI terms adjacent to the modulated signal in each subchannel, i.e.  $q$ . Choi’s method of successive detection with MMSE detection [7] is denoted as Choi’s SDMMSE.

Figure 3.3 shows the BER performances of the mentioned data detection methods when  $f_{nd} = 0.040$ . Due to the assumption of neglecting ICI, the single tap equalization suffers from severe ICI effects and has the worst performance of all. The LS detection has a better performance than single tap equalization. However, the performance degradation of the LS detection increases in high SNR environments. Jeon’s method of LS detection suffers from less noise enhancement than LS detection but more ICI effect than LS detection. It also can be found that Jeon’s method of LS detection has worse performance than that of the ICI cancellation with 3 detection iterations when considering the 4 most dominant ICI terms closest to the modulated signal in each subchannel,  $q = 4$ , in high SNR case. Comparatively, after 3 iterations, the performance of ICI cancellation method is better than the first four methods when SNR is lower than 40dB. However, when SNR is up to 40 dB, some ICI terms cannot be perfectly cancelled due to the errors of the demodulated symbols. Thus, the error

propagation dominates the performance of the ICI cancellation method and an error floor appears. Due to utilizing the time diversity provided by time-selective channels, Choi's method of successive detection with MMSE detection outperforms the other mentioned methods and the reference of the ICI-free. This benefit is more apparent in high SNR case.

Figure 3.4 illustrates the BER performances of the mentioned data detection methods when  $f_{nd} = 0.083$ . The single tap equalization suffers from severe ICI effects and still has the worst performance of all. LS detection suffers from noise enhancement which increases as  $f_{nd}$  gets higher because the minimum nonzero singular value of  $\mathbf{G}$  becomes smaller. Jeon's method of LS detection also suffers from severe ICI effect since too many ICI terms are ignored in the detection. Compared to the LS detection, ICI cancellation method is without the noise enhancement problem. However, the error propagation becomes a serious problem for the ICI cancellation method and cannot be ignored even after six iterations. Choi's method of successive detection with MMSE detection still outperforms the other mentioned methods. Because time selectivity of the fading channel with  $f_{nd} = 0.083$  becomes more apparent than that of the channel with  $f_{nd} = 0.040$ , Choi's method obtains more benefits by utilizing time diversity.

In conclusion, those ICI cancellation methods are not good enough to reduce the ICI effect under the targeted channel environments. An irreducible error floor appears in the high SNR environments regardless of the iteration numbers. Although LS detection outperforms the other detection methods, it still suffers severe noise enhancement problem. The performance degradation is too large. Choi's method is a good choice for detection of OFDM systems in the targeted time-varying fading channels. However, the computational complexity of this method is too high.

## 3.2 Existing Channel Estimation Methods

In this section, two conventional channel estimation methods, LS channel estimation and DFT-based channel estimation, for OFDM systems in time-invariant channel are introduced. Then, two existing channel estimation methods, Chen's method of LS channel estimation [6] and Yeh's algorithm of ICI-reduction method [11], based on channel model with linear variation are described. The simulation results show that the performances of these methods are poor when the normalized Doppler frequency,  $f_{nd}$ , is up to 0.08 and that the estimation errors of these methods are too high for the proposed data detection methods.

### 3.2.1 Least-square Channel Estimation

LS channel estimation is widely used for OFDM systems and is the foundation of other advanced channel estimation methods. The advantage of LS channel estimation is that the pilot patterns are the only required information to accomplish the estimation.

In the following analysis of this section, the number of pilot subcarriers in an OFDM symbol is set to  $M$ , and the channel is assumed to be time-invariant. Thus, the received signal after DFT at the  $k$ -th pilot subcarrier is represented as

$$Y(p(k)) = G(k, k)P(k) + N(p(k)) \quad k = 0, 1, 2, \dots, M-1 \quad (3.9)$$

where  $p(k)$  is the position function of the pilot subcarriers and  $P(k)$  is the known pattern transmitted at the  $k$ -th pilot subcarrier. The channel frequency response at the  $k$ -th pilot subcarrier can be roughly estimated by

$$\hat{G}(p(k), p(k)) = \frac{Y(p(k))}{P(k)} = G(p(k), p(k)) + \frac{N(p(k))}{P(k)} \quad (3.10)$$

Then, the channel frequency responses at the other data subcarriers can be estimated by interpolation techniques. Also, the following DFT-based channel estimation is one

kind of the interpolation techniques.

### 3.2.2 DFT-based Channel Estimation

DFT-based channel estimations have been proposed in [13] [14]. These estimations are based on the technique of interpolation in transform domain to accomplish the estimation and with good performances in the case of sample-spaced channel impulse response. FFT algorithms can be utilized to reduce the computational complexity of the transformation. However, there is a restriction on placement of pilot subcarriers for the DFT-based channel estimation.  $M$  pilot subcarriers must be equispaced along frequency direction as shown in Figure 3.5.

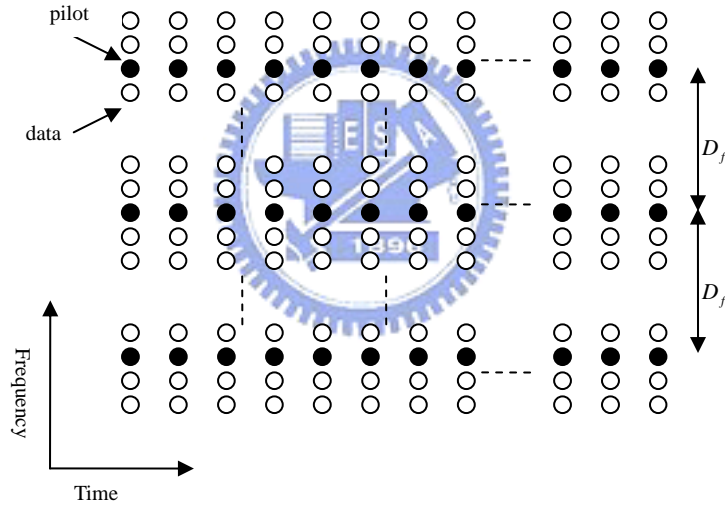


**Figure 3.5** Regular pilot placement [11]

For convenience,  $N/M$  is assumed to be an integer, the first pilot is placed at Subcarrier 0, i.e. D.C, and the channel is assumed to be time-invariant. Therefore, the received signal at the  $k$ -th pilot subcarriers can be expressed as

$$Y(p(k)) = Y\left(\frac{N}{M}k\right) = Y(D_f k), \quad k = 0, 1, 2, \dots, M-1 \quad (3.11)$$

First, the channel frequency response at pilot subcarriers is estimated by LS estimation, i.e. equation (3.10). Observably, the channel frequency response at pilot subcarriers can be viewed as the down-sample of complete frequency response. Then,

$M$ -point IDFT is performed on  $\hat{G}(p(k), p(k))$ .

$$\hat{h}_p(n) = \frac{1}{M} \sum_{k=0}^{M-1} \hat{G}(p(k), p(k)) e^{-j \frac{2\pi nk}{M}}, \quad n = 0, 1, 2, \dots, M-1 \quad (3.12)$$

According to the down sampling theorem, the channel impulse response obtained by  $M$ -point inverse discrete Fourier transform of  $\{G(p(k), p(k)) | k = 0, 1, 2, \dots, M-1\}$  is the overlapped version of the channel impulse response with  $N$  points. For analysis, the maximum path delay time is defined as  $\tau_{\max} t_s$ , and  $\Delta$  is the minimum integer which is larger than  $\tau_{\max}$ . To avoid the aliasing effect, the number of the pilot subcarriers must be larger than the sampled maximum path delay, i.e.  $M > \Delta$ . According to (2.15) and (2.16), the estimation of channel frequency response can be achieved by padding  $N-M$  zeros in the tail of  $\{\hat{h}_p(n) | n = 0, 1, 2, \dots, M-1\}$ ,

$$\hat{h}(n) = \begin{cases} \hat{h}_p(n), & 0 \leq n \leq M-1 \\ 0, & M-1 \leq n \leq N-1 \end{cases} \quad (3.13)$$

and then by performing  $N$ -point DFT on  $\hat{h}(n)$

$$\hat{G}(k, k) = \sum_{n=0}^{N-1} \hat{h}(n) e^{-j \frac{2\pi nk}{N}} \quad k = 0, 1, 2, \dots, N-1 \quad (3.14)$$

### 3.2.3 Chen's Method of Least-square Channel Estimation

Recall the system model described in Section 2.3. The number of the parameters required for estimation in the matrix  $\mathbf{G}$  is  $N^2$  when frequency-domain channel estimation is considered. Apparently, it is impossible to achieve the estimation even if full  $N$  training symbols are transmitted at all  $N$  subcarriers. To make the problem solvable, the number of parameters required for estimation must be reduced to be less than  $N$ . Thus, instead of estimating the channel frequency response, estimating the channel impulse response  $h(n, l)$  is adopted, because the number of channel taps is usually smaller than the number of the subcarriers, i.e.  $L \ll N$ .

Without any assumption, there are still  $LN$  parameters needed for the estimation within an OFDM symbol when the number of channel taps is  $L$ . It is still impossible to achieve the estimation. Fortunately, Jeon et al. [8] stated that the channel variation can be approximated by a straight line when the channel is slowly time-varying (Normalized Doppler frequency,  $f_{nd} < 0.1$ ). This property has been introduced in Section 2.3. Thus, the variation of each channel path can be approximated as [6] [11] [18]

$$\Delta h(n, l) = \left(n - \frac{N-1}{2}\right) \alpha_l \quad (3.15)$$

where  $0 \leq n \leq N-1$ ,  $0 \leq l \leq L-1$ , and  $\alpha_l$  is the slope of the  $l$ -th channel path. Given by (2.15), the response of the  $l$ -th channel path at  $n$ -th time sample can be written as

$$h(n, l) = h_{ave}(l) + \left(n - \frac{N-1}{2}\right) \alpha_l \quad (3.16)$$

Therefore, the number of parameters required for estimation is reduced to  $2L$ . The channel estimation can be achieved by applying least-square (LS) estimation when pilot subcarriers inserted within an OFDM symbol are enough.

Substituting (3.15) into (2.17), the ICI terms of  $\mathbf{G}$  is given by

$$\begin{aligned} G(k, m) &= \frac{1}{N} \sum_{r=0}^{N-1} \sum_{l=0}^{L-1} \left(r - \frac{N-1}{2}\right) \alpha_l e^{\frac{j2\pi r(m-k)}{N}} e^{-\frac{j2\pi lm}{N}} \\ &= -\frac{\sum_{l=0}^{L-1} \alpha_l e^{-\frac{j2\pi ml}{N}}}{1 - e^{-j2\pi(k-m)/N}} = C_{k-m} \mathbf{b}_m^T \boldsymbol{\alpha}, \quad m \neq k \end{aligned} \quad (3.17)$$

where  $\mathbf{b}_m = [1, e^{-j2\pi m/N}, \dots, e^{-j2\pi mL/N}]^T$ ,  $C_{k-m} = -(1 - e^{-j2\pi(k-m)L/N})^{-1}$ , and

$\boldsymbol{\alpha} = [\alpha_0, \dots, \alpha_{L-1}]^T$ . Equation (2.16) can be rewritten as

$$G(k, k) = \mathbf{b}_k^T \mathbf{h}_{ave} \quad (3.18)$$

where  $\mathbf{h}_{ave} = [h_{ave}(0), \dots, h_{ave}(L-1)]^T$ . According to (2.13), the received signal after

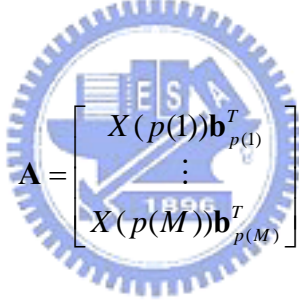
DFT at the  $k$ -th subcarrier is given by

$$\begin{aligned}
Y(k) &= G(k, k)X(k) + \sum_{m=0, m \neq k}^{N-1} G(k, m)X(m) + W(k) \\
&= \mathbf{b}_k^T \mathbf{h}_{ave} X(k) + \underbrace{\sum_{m=0, m \neq k}^{N-1} C_{k-m} \mathbf{b}_m^T \boldsymbol{\alpha} X(m)}_{ICI} + W(k)
\end{aligned} \tag{3.19}$$

By collecting the received signals at all pilot subcarriers, the system model can be expressed as the linear equations

$$\begin{aligned}
\mathbf{Y} &= \begin{bmatrix} Y(p(1)) \\ \vdots \\ Y(p(M)) \end{bmatrix} = \mathbf{A} \mathbf{h}_{ave} + \mathbf{B} \boldsymbol{\alpha} + \mathbf{e} \\
&= [\mathbf{A} \quad \mathbf{B}] \begin{bmatrix} \mathbf{h}_{ave} \\ \boldsymbol{\alpha} \end{bmatrix} + \mathbf{e} \\
&= \mathbf{D} \mathbf{h} + \mathbf{e}
\end{aligned} \tag{3.20}$$

where



$$\mathbf{A} = \begin{bmatrix} X(p(1)) \mathbf{b}_{p(1)}^T \\ \vdots \\ X(p(M)) \mathbf{b}_{p(M)}^T \end{bmatrix} \tag{3.21}$$

$$\mathbf{B} = \begin{bmatrix} \sum_{m \in \text{pilot}, m \neq p(1)} C_{p(1)-m} X(m) \mathbf{b}_m^T \\ \vdots \\ \sum_{m \in \text{pilot}, m \neq p(M)} C_{p(M)-m} X(m) \mathbf{b}_m^T \end{bmatrix} \tag{3.22}$$

$$\mathbf{D} = [\mathbf{A} \quad \mathbf{B}] \tag{3.23}$$

$$\mathbf{h} = \begin{bmatrix} \mathbf{h}_{ave} \\ \boldsymbol{\alpha} \end{bmatrix} \tag{3.24}$$

$$\begin{aligned}
\mathbf{e} &= \begin{bmatrix} e(p(1)) \\ \vdots \\ e(p(M)) \end{bmatrix} \\
&= \begin{bmatrix} \sum_{m=0, m \notin \text{pilot}, m \neq p(1)}^{N-1} C_{p(1)-m} X(m) \mathbf{b}_m^T \\ \vdots \\ \sum_{m=0, m \notin \text{pilot}, m \neq p(M)}^{N-1} C_{p(M)-m} X(m) \mathbf{b}_m^T \end{bmatrix} \boldsymbol{\alpha} + \begin{bmatrix} W(p(1)) \\ \vdots \\ W(p(M)) \end{bmatrix} \quad (3.25)
\end{aligned}$$

where  $p(k)$  is the position function of the pilot subcarriers,  $M$  is the number of the pilot subcarriers, and  $\mathbf{e}$  is composed of noise at the pilot subcarriers and ICI contribution from non-pilot subcarriers. Thus, the estimated channel is obtained by the LS solution of the linear equations from (3.20) when  $M \geq 2L$

$$\hat{\mathbf{h}} = \mathbf{D}^+ \mathbf{Y} \quad (3.26)$$

However, the simulation results (see Section 3.2.5) show that an irreducible error floor still appears in the BER performance when only pilot subcarriers are used for the estimation in the fading channel with  $f_{nd} = 0.083$ , and that this method only takes effect in the all-pilot preamble case.

### 3.2.4 Yeh's Algorithm of ICI-reduction Method

Chen's method of Channel estimation is based on the LS estimation. According to the conclusion in the previous section, this method only takes effect in the all-pilot preamble case. Thus, it is necessary to find out a channel tracking method in the data transmission region where only pilot subcarriers are utilized for the estimation. Yeh [11] proposed a channel tracking method with ICI-reduction technique in linearly-variant fading channels.

Recall the system model described in Section 2.3. The received signal after DFT is given by



$$Y(k) = G(k, k)X(k) + \underbrace{\sum_{m=0, m \neq k}^{N-1} G(k, m)X(m)}_{ICI} + W(k) \quad (3.27)$$

Figure 2.8 shows that the power of  $G(k, k)$  is much larger than the power of  $G(k, m)$  when  $k \neq m$ . Therefore, the channel frequency response at  $k$ -th pilot sub-carrier can be obtained by LS estimation introduced in Section 3.2.1

$$\hat{G}(p(k), p(k)) = \frac{Y(p(k))}{P(k)} = G(p(k), p(k)) + \frac{\sum_{m=0, m \neq k}^{N-1} G(k, m)X(m) + W(k)}{P(k)} \quad (3.28)$$

The second term on the right hand side of (3.28) represents the estimation error and increases as normalized Doppler frequency,  $f_{nd}$ , becomes large. According to (2.16), the estimation of  $h_{ave}(l)$  can be obtained by DFT-based channel estimation introduced in Section 3.2.2

$$\hat{h}_{ave}(l) = \frac{1}{M} \sum_{k=0}^{L-1} \hat{G}(p(k), p(k)) e^{\frac{j2\pi lk}{M}} \quad (3.29)$$

Besides, (3.15) shows that  $h_{ave}(l)$  is the channel impulse response at the midpoint of the symbol interval when channel variation is approximated to linear fashion, i.e.

$h(n = \frac{N-1}{2}, l) = h_{ave}(l)$ . In order to estimate the slopes,  $\alpha_l$ 's, of the channel paths

within single OFDM symbol by using the two  $h_{ave}(l)$ 's of the two consecutive OFDM symbols, it is assumed that channel variation within the two consecutive OFDM symbols is linear, i.e.  $f_{nd} \leq 0.05$ . Therefore, the slopes of the channel paths can be obtained by

$$\hat{\alpha}_l^i = \frac{\hat{h}_{ave}^i(l) - \hat{h}_{ave}^{i-1}(l)}{N + N_{CP}} \quad (3.30)$$

where  $\alpha_l^i$  denotes the slope of the  $l$ -th channel path of the  $i$ -th symbol,  $h_{ave}^i(l)$  denotes the average response of the  $l$ -th channel path of the  $i$ -th symbol, and  $N_{CP}$  denotes the length of the cyclic prefix (CP). This concept is shown in Figure 3.6. The solid line and the dashed line represent the response of one channel path and the cor-

responding estimated response, respectively. The estimation error is the region between the solid line and the dashed line.

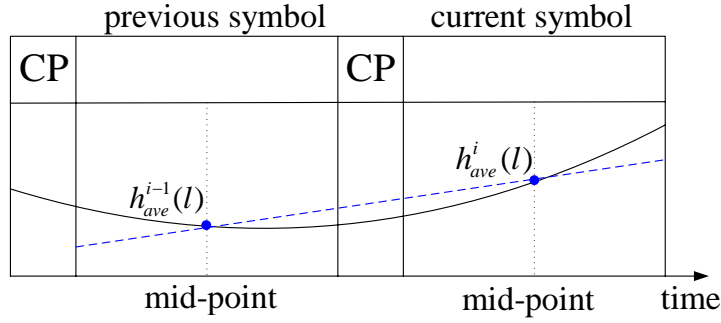


**Figure 3.6** Linear model between two consecutive OFDM symbols [18]

Thus, the ICI terms in (3.19) can be cancelled by using the estimation of the slope,  $\hat{\alpha}_l^i$ , and the demodulated data,  $\hat{X}(k)$ .

The whole procedure of Yeh's method is shown in Figure 3.7 modified from [11].  $I$  represent the iteration number.  $I_{\max}$  is the number of the iterations. In the first iteration, the estimation  $\hat{h}_{ave}^i(l)$  of  $h_{ave}^i(l)$  suffers from whole ICI and has large error. Thus, there are still many erroneous data after demodulation. After several iterations, the ICI terms at the pilot subcarriers would be mitigated by the ICI cancellation procedure. The estimation error of  $\hat{h}_{ave}^i(l)$  becomes small. A more reliable slope of the channel path  $\hat{\alpha}_l^i$  is obtained. The ICI terms at the data subcarriers would be cancelled more clearly. Therefore, the error floor is reduced.

Although Yeh's method operates well in the aspect of the performance and the computational complexity, it is only feasible in the assumption circumstance with  $f_{nd} \leq 0.05$ . Therefore, this method needs some modification to operate in the targeted fast fading channels. Besides, the performance of this method is bounded by the ICI cancellation method with ideal channel state information, i.e. ICI cancellation in Figure 3.3 and Figure 3.4.

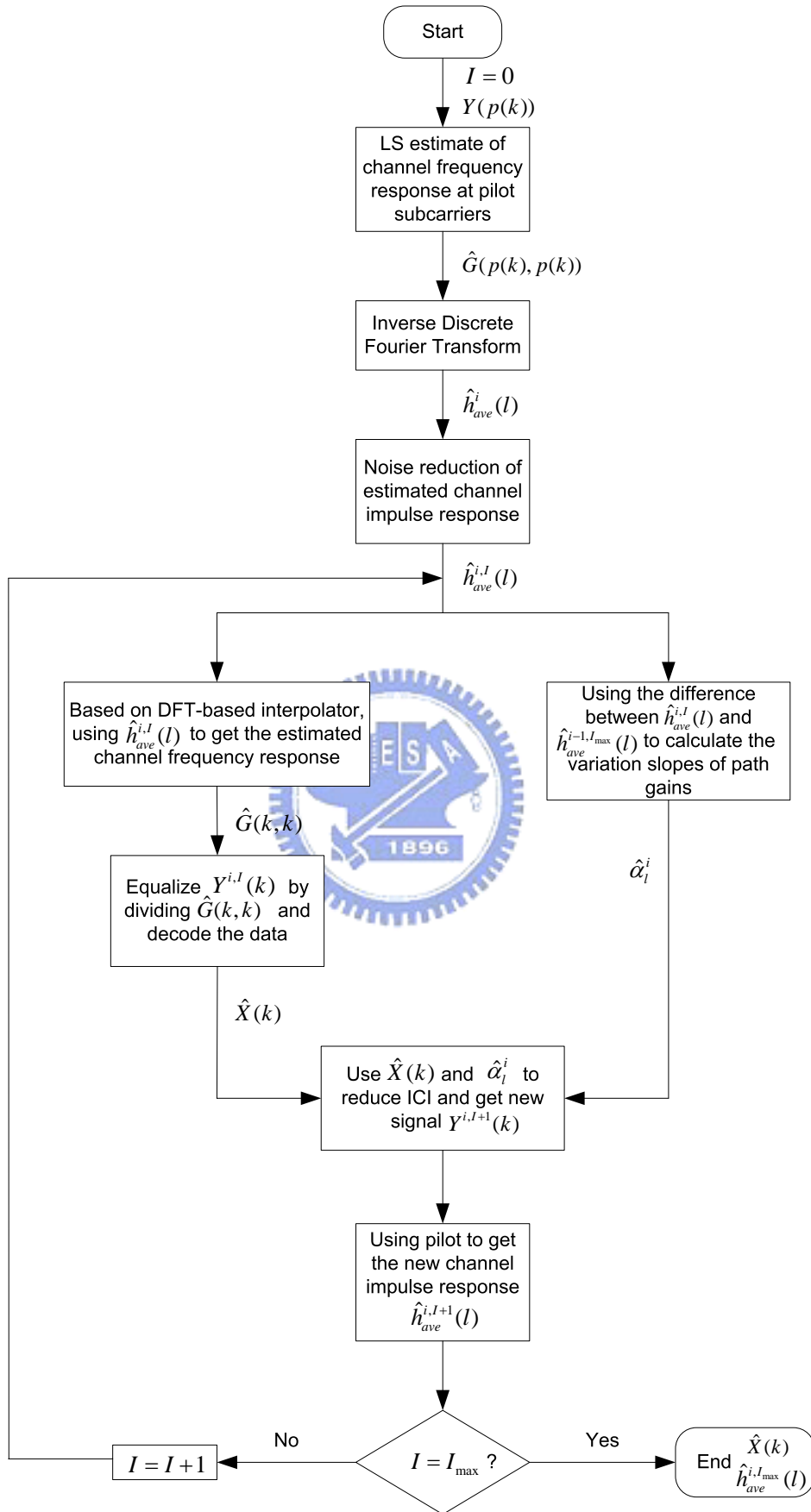


Figure 3.7 Yeh's algorithm of ICI-reduction method [11]

### 3.2.5 Simulation Results

In this section, the performances of the last two mentioned channel estimation methods are evaluated by computer simulations. Multipath Rayleigh fading channels in the simulations are generated by the modified Jakes' model [9] [10]. The power delay profile is chosen as the "Vehicular A" channel model defined by ETSI for the evaluation of UMTS radio interface proposals [17]. The simulated OFDM system parameters and the channel parameters are listed in Table 3.2 and Table 3.3, respectively. The 16 pilot subcarriers grouped into 4 groups are equispaced onto the DFT grid, i.e. the indices of the pilot subcarriers are {0, 1, 2, 3, 16, 17, 18, 19, 32, 33, 34, 35, 48, 49, 50, 51} within 64 subcarriers. These pilot patterns are used for Chen's method of LS channel estimation. For Yeh's algorithm of ICI reduction method, the 16 pilot subcarriers are equispaced along frequency direction, i.e. the indices of the pilot subcarriers are {0, 4, 8, 12, 16, 20, 24, 28, 32, 36, 40, 44, 48, 52, 56, 60} within 64 subcarriers, due to DFT-based channel estimation. Beside, an all-pilot preamble is attached in front of the data symbols for the initial channel estimation. It is assumed that the maximum path delay time is known at the receiver and that synchronization is perfect.

**Table 3.2** Simulated OFDM system parameters

Operating frequency	3.5GHz
Signal bandwidth	2.5MHz
FFT length	64
Number of pilot subcarriers	16
Number of data subcarriers	48
Symbol duration	25.6us
Subcarrier spacing	39.1kHz
Modulation	QPSK
Channel coding	No
Power delay profile	ETSI Vehicular A
Normalized Doppler frequency	0.083 and 0.040

**Table 3.3** ETSI Vehicular A channel environment

Tap	Relative delay (ns)	Average power (dB)
1	0	0.0
2	310	-1.0
3	710	-9.0
4	1090	-10.0
5	1730	-15.0
6	2510	-20.0

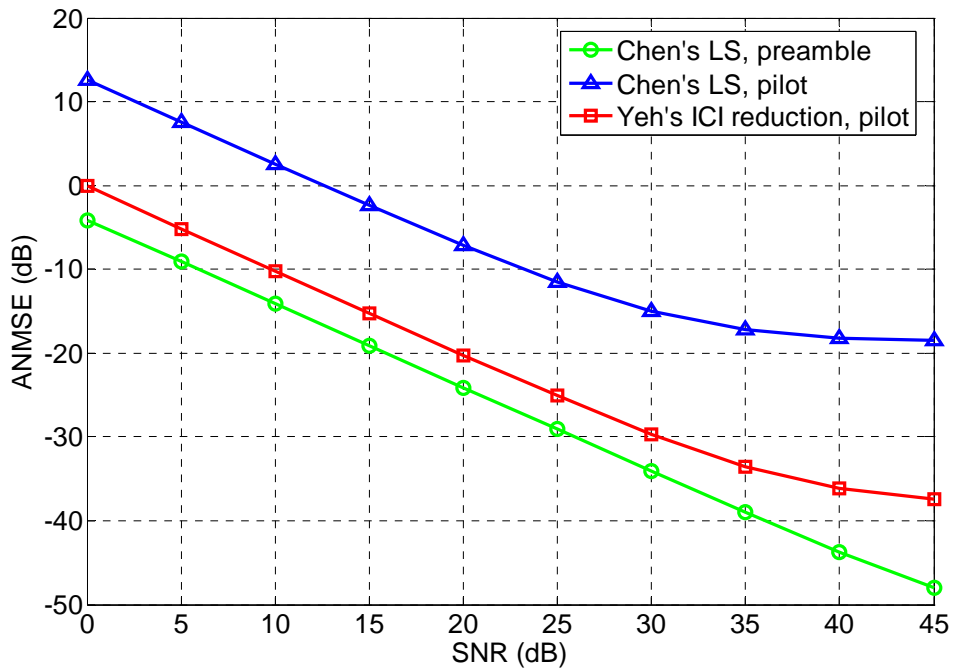


**Figure 3.8** ANMSE performances of Chen's and Yeh's methods of channel estimation in the "Vehicular A" channel with  $f_{nd} = 0.040$

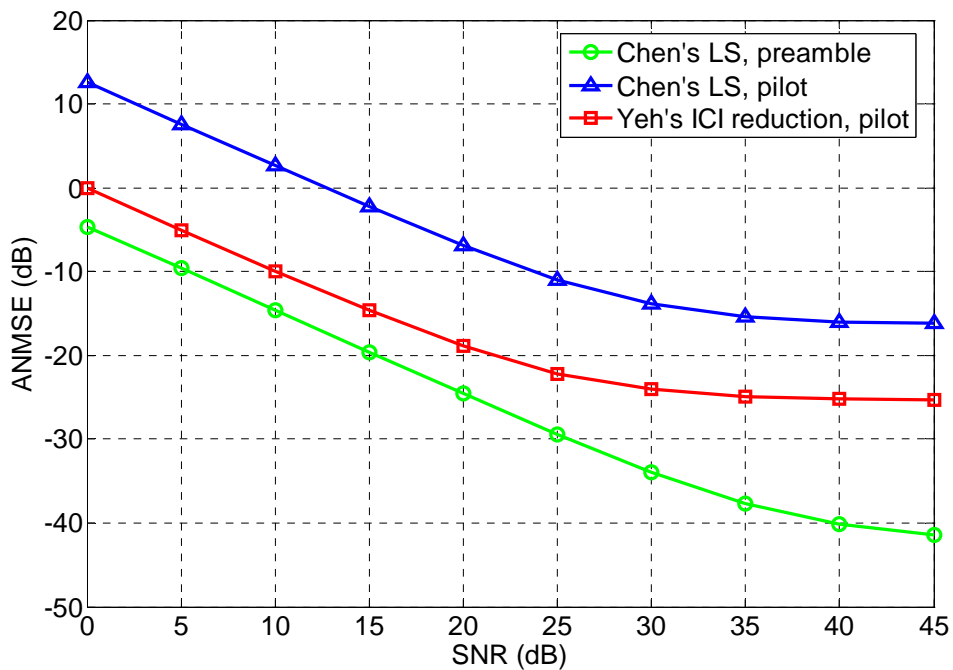


**Figure 3.9** ANMSE performances of Chen's and Yeh's methods of channel estimation in the "Vehicular A" channel with  $f_{nd} = 0.083$

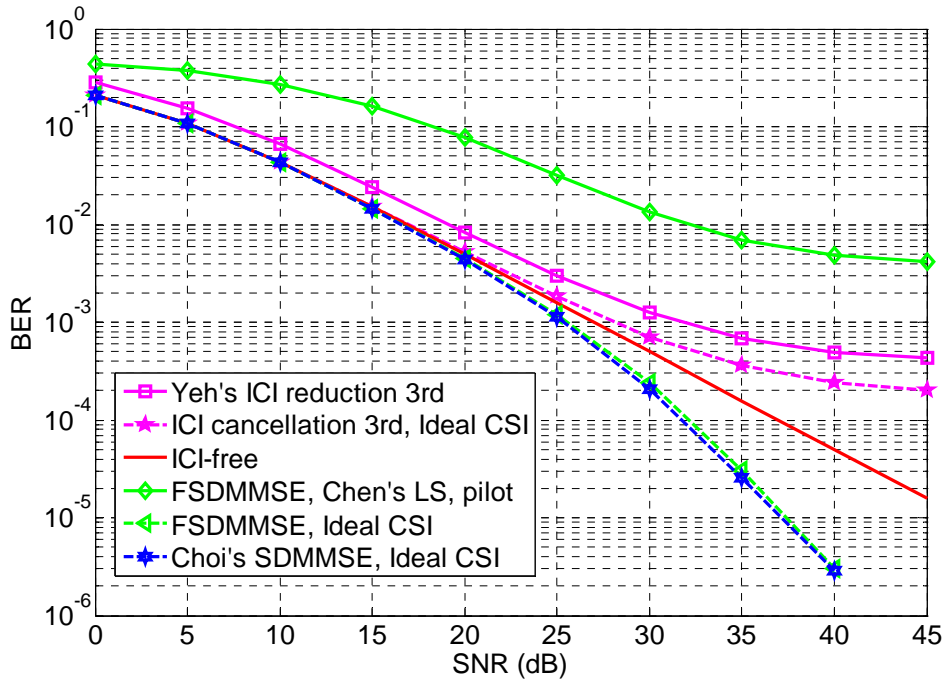


**Figure 3.10** BER performances of Chen's and Yeh's methods of channel estimation combined with data detection methods in the "Vehicular A" channel with  $f_{nd} = 0.040$

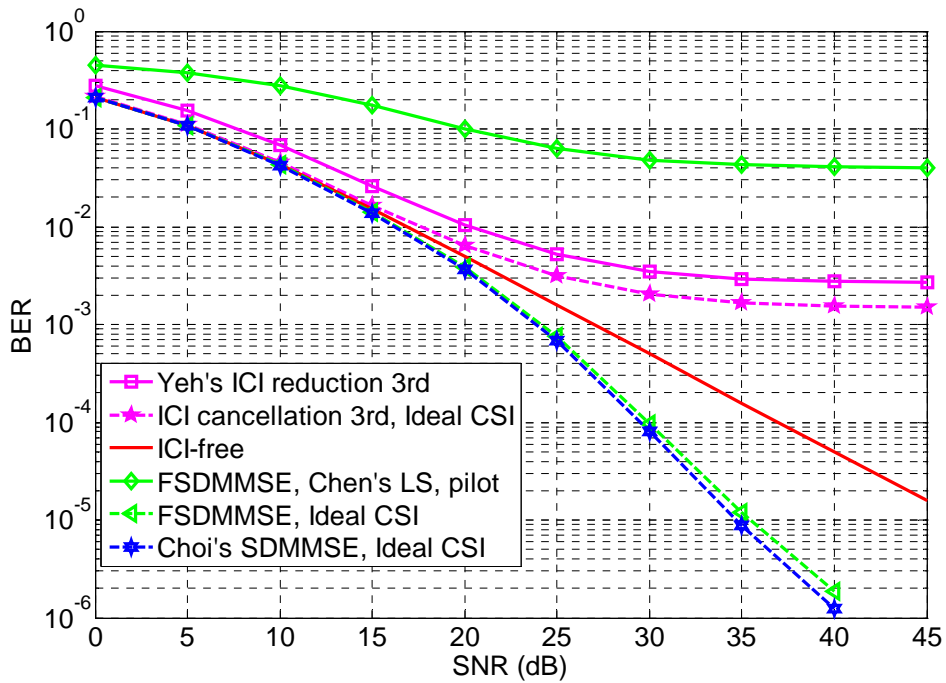


**Figure 3.11** BER performances of Chen's and Yeh's methods of channel estimation combined with data detection methods in the "Vehicular A" channel with  $f_{nd} = 0.083$

In Figure 3.8 and Figure 3.9, ANMSE indicates the average normalized mean square error, which is defined as

$$ANMSE = \frac{1}{N_{sym}} \sum_{i=1}^{N_{sym}} \left\{ \frac{\sum_{k=0}^{N-1} \sum_{m=0}^{N-1} |G^i(k, m) - \hat{G}^i(k, m)|^2}{\sum_{k=0}^{N-1} \sum_{m=0}^{N-1} |G^i(k, m)|^2} \right\} \quad (3.31)$$

where  $N_{sym}$  is the number of the transmitted OFDM symbols,  $\hat{G}^i(k, m)$  is the estimation of  $G^i(k, m)$ , and  $G^i(k, m)$  is the channel frequency response within the  $i$ -th OFDM symbol defined in Section 2.3. The terms “Chen’s LS, preamble” and “Chen’s LS, pilot” indicate that Chen’s methods of LS channel estimation, introduced in Section 3.2.3, are applied to the all-pilot preamble and the pilot subcarriers, respectively. The term “Yeh’s ICI reduction, pilot” indicates that Yeh’s algorithm of ICI reduction method [11] with 3 detection iterations, introduced in Section 3.2.4, is applied to the pilot subcarriers.

In Figure 3.10 and Figure 3.11, the term “ICI-free” indicates the theoretical BER performance of the coherent detection in the time-invariant flat Rayleigh fading channel for the reference of the ICI-free case. The ordinal numbers appended to “ICI cancellation” and “Yeh’s ICI reduction” indicate the numbers of the iterations performed in the two methods. The terms “FSDMMSE” and “Choi’s SDMMSE” indicate that the proposed frequency-domain successive detection method with MMSE detection (see Section 4.1) and Choi’s method of successive detection with MMSE detection [7] are adopted in data detection, respectively. The term “Ideal CSI” indicates that ideal channel state information is applied to data detection.

Figure 3.8 and Figure 3.9 illustrate ANMSE performances of Chen’s and Yeh’s methods of channel estimation in the “Vehicular A” channel with  $f_{nd} = 0.040$ , and  $f_{nd} = 0.083$ , respectively. Chen’s method applied to the all-pilot preamble has the least channel estimation error of all. It can be viewed as the performance boundary of



Chen's method applied to any other pilot pattern when the number of pilot subcarriers is less than  $N$ . Apparently, the performance degradation of Chen's method applied to the pilot subcarriers is very large. Under the same ANMSE condition, Yeh's method with 3 detection iterations applied to the pilot subcarriers has about 4~5dB performance loss compared to Chen's method applied to the all-pilot preamble when  $f_{nd} = 0.040 \sim 0.083$ . Besides, the channel estimation errors of these methods increase as  $f_{nd}$  becomes large, especially in the high SNR case.

Figure 3.10 and Figure 3.11 illustrate the BER performances of Chen's and Yeh's methods of channel estimation combined with data detection methods in the "Vehicular A" channel with  $f_{nd} = 0.040$ , and  $f_{nd} = 0.083$ , respectively. Because of the large channel estimation error, Chen's method applied to the pilot subcarriers combined with the proposed detection method has the worst performance of all. There is a large performance degradation compared to the proposed detection method with ideal channel state information. As known in Section 3.2.4, the performance of Yeh's method is bounded by the ICI cancellation method with ideal channel state information.

In conclusion, the Yeh's method is not good enough to reduce the ICI effect under the targeted channel environments. The channel estimation error of the Chen's method applied to the pilot subcarriers is too large for the proposed detection methods. Thus, it is necessary to develop more reliable channel estimation.

## Chapter 4

# The Proposed Data Detection and Channel Estimation Methods



In the previous chapter, some existing data detection and channel estimation methods are described, briefly. However, the simulation results show that these methods except Choi's method of successive detection are not effective in the time-varying environments, where normalized Doppler frequency,  $f_{nd}$ , is up to 0.08. Based on the concepts of the mentioned methods [6] [7] [8] [11], modified data detection and channel estimation methods are proposed for the targeted channel environments. The computational complexities of the proposed methods and their introduced additional costs are also discussed.

### 4.1 The Proposed Frequency-domain Successive Detection Methods

As mentioned in the previous chapter, the computational complexity of Choi's method of successive detection is too high to be realized. Fortunately, some properties of the time-varying fading channels described in Section 2.3 combined with the technique introduced in Section 3.1.3 help to reduce the computational complexity of the successive detection method and make the method feasible.

#### 4.1.1 Algorithms of the Frequency-domain Successive Detection Methods

In order to exploit time diversity involved in time-selective fading channels, Choi et al. proposed their successive detection method performing in the time domain, intuitively. However, in most-considered application environments, the correlation of the channel impulse response within OFDM symbol duration is still high. It is hard to predict which time samples suffer less fading effect and only to process these time samples for better efficiency. Besides, since the modulated signals transmitted in different subchannels are mixed in the time domain, the whole  $N$  received time samples must be used for the separation of modulated signals from the received signal without additional ICI induced by the non-periodic DFT windows. Thus, no special properties of the system model in the time domain can be utilized to reduce the computational complexity.

Fortunately, some properties of the channel frequency response can help reduce the computational complexity of the successive detection method. First, Parseval's Theorem states that average power of the signal in time equals sum of average power of the signal in the  $k$ -harmonics, i.e. power conservation property.

$$\frac{1}{N} \sum_{n=0}^{N-1} |h(n, l)|^2 = \sum_{k=0}^{N-1} |T(k, l)|^2 \quad (4.1)$$

where  $T(k, l) = \sum_{n=0}^{N-1} h(n, l) e^{-j2\pi kn/N}$ . Therefore, the power gain of time diversity obtained

in the frequency domain is the same as that obtained in the time domain.

Second, recall the system model shown in Section 2.3. The received signal after DFT is represented as

$$\mathbf{Y} = \mathbf{G}\mathbf{X} + \mathbf{W} \quad (2.19)$$

The successive detection is modified to perform in the frequency domain. According to the properties mentioned in Section 3.1.3, the power of the time-varying fading channel is compressed by DFT, i.e. most power of the time-varying fading channel concentrates in the neighborhood of subcarriers and does not spread over the spectrum. Consequently, the computation of linear detection in Step P-1 in Figure 3.2 is changed from pseudo inversion of the  $N \times N$  matrix  $\mathbf{G}$  to  $N$  pseudo inversions of the  $(q+1) \times (q+1)$  matrices  $\mathbf{G}_{blk,k}$ . Hence, the computational complexity of the linear detection in Step P-1 is reduced from  $O(N^3)$  to  $O(N(q+1)^3)$ . Thus, by utilizing these two properties, the successive detection performing in the frequency domain not only gains time diversity but also has lower computational complexity.

There are additional benefits when the successive detection performs in the frequency domain. Only the pseudo inversions and the norms of the corresponding equalization vectors of the subcarriers adjacent to the demodulated subcarrier in the current detection layer are necessarily updated for the proposed methods with LS detection, which is shown in Step P-5 and Step P-6 in Figure 4.1. This property can also be applied for the signal to interference and noise ratio (SINR) calculation of the proposed methods with MMSE detection. Therefore, the computational complexity can be further reduced. The complexity analysis is detailed in Section 4.1.2. The structures of  $\mathbf{G}_{blk,k}$ 's are depicted in Figure 3.1.

The proposed detection methods proceed as follows:

Least Square (LS) Version
---------------------------

$$j = 1$$

$$\mathbf{U}_{blk,k}^H = \mathbf{G}_{blk,k}^+ \quad 0 \leq k \leq N-1 \quad (P-1)$$

$$i_1 = \arg \min_k \left\| \mathbf{u}_{blk,k,q/2+1} \right\|^2 \quad (P-2)$$

Loop

$$z(i_j) = \mathbf{u}_{blk,i_j,q/2+1}^H \mathbf{Y}_{blk,i_j} \quad (P-3)$$

$$\hat{X}(i_j) = \text{slice}(z(i_j))$$

$$\mathbf{Y} = \mathbf{Y} - \mathbf{g}_{i_j} \hat{X}(i_j) \quad (P-4)$$

$$\mathbf{G} = [\mathbf{g}_0, \dots, \mathbf{g}_{i_j-1}, \mathbf{0}, \mathbf{g}_{i_j+1}, \dots, \mathbf{g}_{N-1}]$$

$$\mathbf{U}_{blk,k}^H = \mathbf{G}_{blk,k}^+ \quad (P-5)$$

$k \in \{i_j - q/2, \dots, i_j - 1, i_j + 1, \dots, i_j + q/2\}$

$$i_{j+1} = \arg \min_{k \notin \{i_1, \dots, i_j\}} \left\| \mathbf{u}_{blk,k,q/2+1} \right\|^2 \quad (P-6)$$

$$j = j + 1$$

Minimum Mean Square Error (MMSE) Version
--

$$j = 1$$

$$\mathbf{U}_{blk,k}^H = (\mathbf{G}_{blk,k}^H \mathbf{G}_{blk,k} + \sigma^2 \mathbf{I})^{-1} \mathbf{G}_{blk,k}^H, \quad 0 \leq k \leq N-1 \quad (P-1)$$

$$i_1 = \arg \max_k SINR_k = \arg \max_k \frac{\left| \left\langle \mathbf{u}_{blk,k,q/2+1}, \mathbf{g}_{blk,k,q/2+1} \right\rangle \right|^2}{\sum_{m, m \neq q/2+1} \left| \left\langle \mathbf{u}_{blk,k,q/2+1}, \mathbf{g}_{blk,k,m} \right\rangle \right|^2 + \sigma^2 \left\| \mathbf{u}_{blk,k,q/2+1} \right\|^2} \quad (P-2)$$

Loop

$$z(i_j) = \mathbf{u}_{blk,i_j,q/2+1}^H \mathbf{Y}_{blk,i_j} \quad (P-3)$$

$$\hat{X}(i_j) = \text{slice}(z(i_j))$$

$$\mathbf{Y} = \mathbf{Y} - \mathbf{g}_{i_j} \hat{X}(i_j) \quad (P-4)$$

$$\mathbf{G} = [\mathbf{g}_0, \dots, \mathbf{g}_{i_j-1}, \mathbf{0}, \mathbf{g}_{i_j+1}, \dots, \mathbf{g}_{N-1}]$$

$$\mathbf{U}_{blk,k}^H = (\mathbf{G}_{blk,k}^H \mathbf{G}_{blk,k} + \sigma^2 \mathbf{I})^{-1} \mathbf{G}_{blk,k}^H \quad (P-5)$$

$k \in \{i_j - q/2, \dots, i_j - 1, i_j + 1, \dots, i_j + q/2\}$

$$i_{j+1} = \arg \max_{k \notin \{i_1, \dots, i_j\}} \frac{\left| \left\langle \mathbf{u}_{blk,k,q/2+1}, \mathbf{g}_{blk,k,q/2+1} \right\rangle \right|^2}{\sum_{m, m \neq q/2+1} \left| \left\langle \mathbf{u}_{blk,k,q/2+1}, \mathbf{g}_{blk,k,m} \right\rangle \right|^2 + \sigma^2 \left\| \mathbf{u}_{blk,k,q/2+1} \right\|^2} \quad (P-6)$$

$$j = j + 1$$

**Figure 4.1** The proposed frequency-domain successive detection methods

In the proposed methods,  $\mathbf{u}_{blk,k,q/2+1}$  and  $\mathbf{g}_{blk,k,q/2+1}$  are the *middle* column vectors of the matrices  $\mathbf{U}_{blk,k}$  and  $\mathbf{G}_{blk,k}$ , respectively.  $q$  is the number of the dominate ICI terms.  $\mathbf{g}_{blk,k,m}$  is the  $m$ -th column vector of the matrix  $\mathbf{G}_{blk,k}$ .  $\mathbf{G}_{blk,k}$  and  $\mathbf{Y}_{blk,k}$  are the  $k$ -th submatrix of the matrices  $\mathbf{G}$  and  $\mathbf{Y}$ , obtained from Section 3.1.3, respectively.  $\mathbf{g}_k$  is the  $k$ -th column vector of the matrix  $\mathbf{G}$ .

### 4.1.2 Complexity Analysis

The proposed data detection methods are modified from Choi's method for lowering computational complexity. Thus, the complexity reductions in the main procedures of the proposed methods are indicated precisely in the following analysis. Also, the computational complexities of other mentioned methods are shown for comparison. Besides, the memory requirements for the two successive detection methods are analyzed and compared. In the end of the section, additional efforts and drawbacks for the proposed data detection methods are discussed. Here, the proposed methods with LS detection are only considered in the following analysis. Also, the proposed methods with MMSE detection can be analyzed in the same way.

### Complexity Reduction

Because it is hard to calculate the counts of the computational operations of the proposed detection methods precisely, the first and last detection layers of the two methods are only considered and compared instead. If we can make sure that the counts of the computational operations of the proposed detection methods are less than that of Choi's method in these two detection layers, we can claim that the proposed detection method has less computational complexity than Choi's method. However, the difference between the two successive detection methods in the last

layer is only Step P-3. It is easy to show that the proposed methods have the less computational complexity. For more serious analysis, the detection layers before the last detection layers of the two successive detection methods are considered instead.

By comparison of Choi's method and the proposed methods shown in Figure 3.2 and Figure 4.1 respectively, the quantities of complexity reduction of the proposed methods in the first detection layer are listed in the descending order as: [16]

- Computational complexity of the pseudo inversion in Step P-1 is reduced from  $O(N^3)$  to  $O(N(q+1)^3)$ .
- Computational complexity of updating the pseudo inversion in Step P-5 is reduced from  $O(N(N-1)^2)$  to  $O(q(q+1)q^2)$ .
- Computational complexity of the norm operation of the equalization vector in Step P-2 and Step P-6 is reduced from  $O(N^2)$  to  $O((q+1)^2)$ .
- The number of norms of the updated equalization vectors in Step P-6 is reduced from  $N-1$  to  $q$ .
- Taps of the equalization vectors in Step P-3 is reduced from  $N$  to  $(q+1)$ .

The counts of the computational operations of the proposed and Choi's successive detection methods in the first layered detection are shown in Table 4.1, clearly. In the following tables, the numbers of the complex divisions, multiplications, and additions are listed, respectively. Gaussian elimination is adopted for the matrix inversion [19]. It is assumed that the matrix inversions in the detection procedures all exist.

The quantities of the complexity reduction of the proposed methods in the detection layer before the last one are listed in the descending order as

- Computational complexity of updating the pseudo inversion in Step P-5 is reduced from  $O(N^2)$  to  $O(2(q+1)2^2)$  or to  $O(2(q+1))$ .
- Computational complexity of the norm operation of the equalization vector in Step P-6 is reduced from  $O(N^2)$  to  $O((q+1)^2)$ .

- Taps of the equalization vectors in Step P-3 is reduced from  $N$  to  $(q+1)$ .

The counts of the computational operations of the proposed and Choi's successive detection methods in the detection layer before the last one are shown in Table 4.2.

**Table 4.1** Complexity statistics of the proposed and Choi's successive detection methods in the first detection layer

	# of divisions	# of multiplications	# of additions
Choi's method [7]	$2N^2 - 4N + 2$	$6N^3 - 7N^2 + 8N - 2$	$6N^3 - 11N^2 + 9N - 3$
Proposed method	$(q+1)^3 + (N-4)(q+1)^2 + (5-N)(q+1) - 2$	$3(q+1)^4 + (3N-11)(q+1)^3 + (16-N)(q+1)^2 + (N-9)(q+1) + N + 2$	$3(q+1)^4 + (3N-13)(q+1)^3 + (17-3N)(q+1)^2 + (N-10)(q+1) + 3$

**Table 4.2** Complexity statistics of the proposed and Choi's successive detection methods in the detection layer before the last one

	# of divisions	# of multiplications	# of additions
Choi's method [7]	2	$12N + 4$	$10N - 3$
Proposed method	4 or 2	$19(q+1) + N$ or $7(q+1) + N$	$15(q+1) + N - 3$ or $5(q+1) + N - 5$

**Table 4.3** Complexity statistics of the proposed and Choi's successive detection methods in the first detection layer with  $N = 64$ , and  $q=8, 4$

		# of divisions	# of multiplications	# of additions
Choi's method [7]		7938	1544702	1528381
Proposed method	$q = 8$	5056	156081	164838
	$q = 4$	1328	26041	28898
Reduction %	$q = 8$	36.31%	89.90%	89.21%
	$q = 4$	83.27%	98.31%	98.11%



**Table 4.4** Complexity statistics of the proposed and Choi's successive detection methods in the detection layer before the last one with  $N = 64$ , and  $q = 8, 4$

		# of divisions	# of multiplications	# of additions
Choi's method [7]		2	772	637
Proposed method	$q = 8$	4 or 2	235 or 127	196 or 104
	$q = 4$	4 or 2	159 or 99	136 or 84
Reduction %	$q = 8$	0% or 0%	69.56% or 83.55%	69.23% or 83.67%
	$q = 4$	0% or 0%	79.40% or 87.18%	78.65% or 86.81%

The complexity statistics of the proposed and Choi's successive detection methods in the targeted simulation environments are shown in Table 4.3 and Table 4.4. The percentages of complexity reductions of the proposed methods compared with Choi's method are listed in the bottoms of the tables.

Table 4.3 shows that the reduction percentages of the multiplication and the addition operations of the proposed methods is roughly up to 90% in the first layered detection even if  $q = 8$ . However, the reduction of the divisions is relatively small because the number of divisions is proportional to  $O(N^2)$  not  $O(N^3)$ . The computational complexity of updating the matrix inversion of the proposed methods in the succeeding layered detection gradually approaches that of Choi's method, because the dimensions of matrices for inversions in Choi's method become small. Therefore, the benefits for utilizing the spare matrix structure of Jeon's LS method decrease. In Table 4.4, the reduction percentages of the multiplication and the addition operations of the proposed methods drop to 70% in the detection layer before the last one. Unfortunately, additional divisions for the matrix inversions of the block matrices are required when un-demodulated signals gather together. In conclusion, it is supposed that the percentages of the complexity reductions excluding divisions of the proposed detec-

tion methods with  $q = 8$  and  $q = 4$  are at least 75% and 85%, respectively.

The computational complexities of the other mentioned methods are shown in Table 4.5, where  $I$  indicates the number of the iterations of the ICI cancellation method. The ratios of the computational complexities of different data detection methods to that of Choi's method in the first detection layer in the targeted simulation environments are shown in percentage in Table 4.6. The percentages of complexity ratios of the proposed methods only include the computational operations in the first detection layer, because it is hard to evaluate the exact computational operations of the proposed methods.

**Table 4.5** Complexity statistics of the other mentioned methods

	# of divisions	# of multiplications	# of additions
LS detection	$N^2 - N$	$N^3$	$3N^3 - 2N^2 - N$
ICI cancellation	$I \times N$	$I \times (N^2 - N)$	$I \times (N^2 - N)$
Jeon's LS [8]	$N(q+1)^2 - N(q+1)$	$3N(q+1)^3 - N(q+1)^2 + N(q+1)$	$3N(q+1)^3 - 3N(q+1)^2 + N(q+1) - N$

**Table 4.6** Complexity ratio % of the detection methods  $N = 64$ ,  $q = 8, 4$  and,  $I = 3$

Complexity ratio %		Division	Multiplication	Addition
LS detection		50.79%	50.91%	50.92%
ICI cancellation		2.42%	0.78%	0.79%
Jeon's LS [8] ( $q = 4$ )		16.13%	1.47%	1.27%
Proposed method	$q = 4$	16.73%	1.69%	1.89%
	$q = 8$	63.69%	10.10%	10.79%

In Table 4.6, it is known that the ICI cancellation method with 3 detection iterations has the least computational complexity of all the compared detection methods. For achieving whole detection, the numbers of the multiplication and addition operations are less than 1% those of Choi's method in the first layered detection. Jeon's method of LS detection with a worse performance than that of the ICI cancellation method with 3 detection iterations, however, is more than 1.5 times the numbers of the multiplications and additions of the ICI cancellation method with 3 detection iterations. The computational complexity of the proposed method with  $q = 4$  is larger than those of Jeon's method of LS detection and ICI cancellation method with 3 detection iterations. It is noted that the percentages of complexity ratios of the proposed methods shown in Table 4.6 only include the computational operations in the first detection layer.



## Memory Requirement

The memory requirements for Choi's method are listed as

- $N \times N$  memory cells for  $\mathbf{V}$
- $N \times N$  memory cells for  $\mathbf{U}$
- $N \times 1$  memory cells for  $\mathbf{y}$

The memory requirements for the proposed methods are listed as

- $N \times N$  memory cells for  $\mathbf{G}$
- $N (q+1) \times (q+1)$  memory cells for  $\mathbf{u}_{blk,k,q/2+1}$
- $N \times 1$  memory cells for  $\mathbf{Y}$
- $N$  memory cells for  $\|\mathbf{u}_{blk,k,q/2+1}\|^2$  (optional)

It is noted that  $N$  memory cells for  $\|\mathbf{u}_{blk,k,q/2+1}\|^2$  is not necessary if  $\|\mathbf{u}_{blk,k,q/2+1}\|^2$  for

$k \notin \{i_1, \dots, i_j\}$  is recalculated in each detection layer. In other words, the number of additions and multiplications can be reduced if the norms of the updated  $\mathbf{u}_{blk,k,q/2+1}$ 's in each detection layer are refreshed, only. However,  $N$  memory cells for storing unchanged  $\|\mathbf{u}_{blk,k,q/2+1}\|^2$  is required.

### Additional Control Logic

In order to update the norms and pseudo inversions of the matrices  $\mathbf{G}_{blk,k}$ 's of the subcarriers adjacent to the demodulated signals smartly, additional control logic is required in Step P-5 and Step P-6. Besides, the control logic for block memory access  $\mathbf{G}_{blk,k}$  and  $\mathbf{Y}_{blk,k}$  is demanded in Step P-1, Step P-3 and Step P-5.

Although the proposed methods gain the same time diversity as Choi's method (see Section 5.1) and have much lower computational complexity than Choi's method, it still suffers long system latencies due to the successive detection. This problem becomes severe when the number of the subcarriers is very large. In this case, it would also cause the problem that more dominant ICI terms close to the modulated signal in each subchannel must be considered in the proposed methods. The computational complexities increase so rapidly that the proposed methods can not be easily realized. Moreover, reliable channel estimation is required for the correct detection (see Section 5.2). Finding reliable channel estimation is a real challenge in the following research.

## 4.2 The Proposed Channel Estimation Methods

Recall the simulation results in Section 3.2.5. Chen's method of channel estimation is only feasible in the all-pilot preamble case. Yeh's method only operates properly when  $f_{nd} \leq 0.05$ . Each one of them can not operate in the fast fading channel with  $f_{nd} = 0.083$ . Thus, the modification of Yeh's method is proposed for more reliable channel tracking when  $f_{nd} = 0.083$ . Then, a hybrid method of channel estimation is proposed for the initial channel estimation and the proceeding channel tracking.

### 4.2.1 Modification of Yeh's ICI-reduction Method

In Yeh's method, the slope of the channel impulse response within single OFDM symbol is estimated from the two  $h_{ave}(l)$ 's of the two consecutive OFDM symbols. However, the channel variation during two consecutive OFDM symbols is not linear when  $f_{nd} > 0.05$ . Thus, a modification is given and shown in Figure 4.2. By comparison of Figure 3.6 and Figure 4.2, it shows that the error region of the modified linear model is smaller than that of the original linear model.

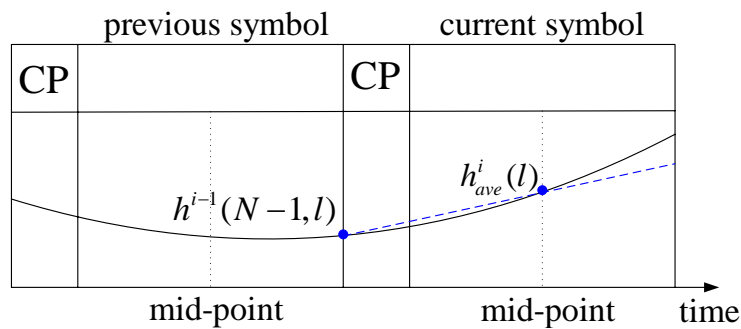


**Figure 4.2** Modified linear model between two consecutive OFDM symbols

The channel impulse response of the previous OFDM symbol at the end of the symbol interval instead of at the midpoint of the symbol interval is utilized for the estimation of the slope of the channel tap,  $\hat{\alpha}_l^i$ . Thus, the slopes of the channel paths can be ob-

tained by

$$\hat{\alpha}_l^i = \frac{\hat{h}_{ave}^i(l) - \hat{h}^{i-1}(N-1, l)}{N/2 + N_{CP}} \quad (4.2)$$

where  $\hat{h}^{i-1}(N-1, l)$  denotes the channel impulse response of the  $l$ -th channel path of the  $(i-1)$ -th symbol at the  $(N-1)$ -th time sample.

#### 4.2.2 The Hybrid LS/ICI-reduction Channel Estimation Method

To obtain reliable initial channel estimation, an all-pilot preamble is attached in front of the data symbols. Chen's method of LS channel estimation is adopted for the channel estimation in the preamble region. Thus, a reliable channel impulse response of the preamble at the end of the symbol interval is obtained. Yeh's ICI-reduction method with the proposed modification is utilized for the channel estimation in the succeeding data symbols. However, the simulation results (see Section 5.3) show that the estimated channel response obtained by the above two procedures is not good enough for the proposed detection methods. It is also known in Section 5.2 that the tolerated channel estimation error for the proposed detection is very small. To reduce the channel estimation error, the demodulated data obtained by the above two procedures are fed to Chen's method of LS channel estimation again. Then, the proposed detection method and the estimated channel response obtained by the second stage of Chen's method of LS channel estimation are used for the detection stage. The whole procedure is shown in Figure 4.3.

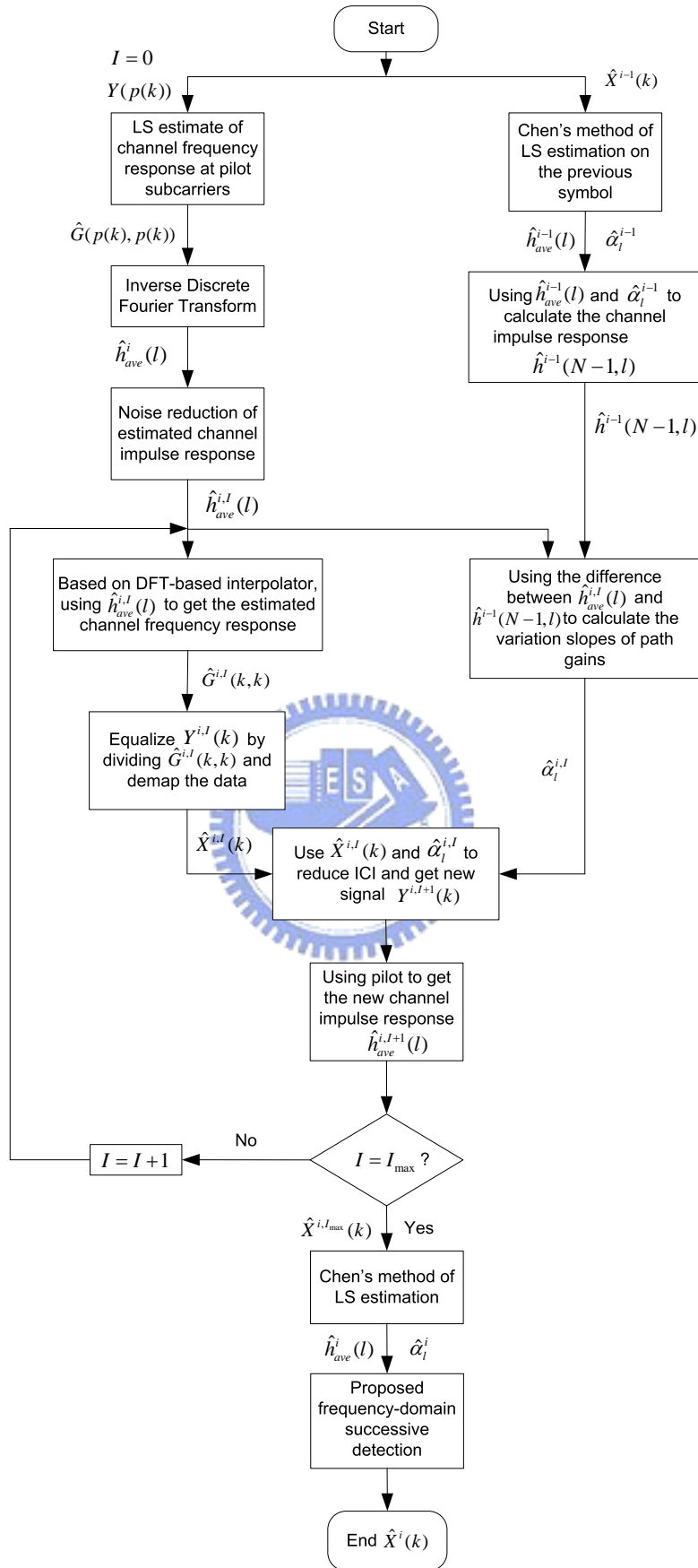


Figure 4.3 Procedure of the proposed channel estimation and data detection

# Chapter 5

## Simulation Results



In this chapter, the performances of the proposed data detection methods and the proposed channel estimation methods are evaluated by computer simulations. The effect of channel estimation errors on the proposed data detection methods is also evaluated by computer simulations. Multipath Rayleigh fading channels in the simulations are generated by the modified Jakes' model [9] [10]. The power delay profile is chosen as the “Vehicular A” channel model defined by ETSI for the evaluation of UMTS radio interface proposals [17]. A two-ray equal power channel model is also considered. For the simulations, the channel power is normalized to 1. The simulated OFDM system parameters and the channel parameters are listed in Table 3.1, Table 3.2, and Table 3.3, respectively.



## 5.1 The Performances of the Proposed Frequency-domain Successive Detection Methods

In this section, it is assumed that perfect channel state information is known at the receiver and that synchronization is perfect. In Figure 5.1~Figure 5.4, the term “ICI-free” indicates the theoretical BER performance of the coherent detection in the time-invariant flat Rayleigh fading channel for the reference of the ICI-free case. The terms “FSDLS” and “FSDMMSE” indicate the proposed frequency-domain successive detection methods with LS detection and with MMSE detection, respectively. The terms “ $q$ =number” appended to “FSDLS”, “FSDMMSE”, and “Jeon’s LS” indicate the number of the dominant ICI terms adjacent to the modulated signal in each subchannel, i.e.  $q$ . Jeon’s method of LS detection [8] is denoted as Jeon’s LS. The ordinal numbers appended to ICI cancellation indicate the number of the iterations performed in the ICI cancellation method. The performances of the proposed data detection methods are bounded by Choi’s method of successive detection with MMSE detection [7], denoted as Choi’s SDMMSE.

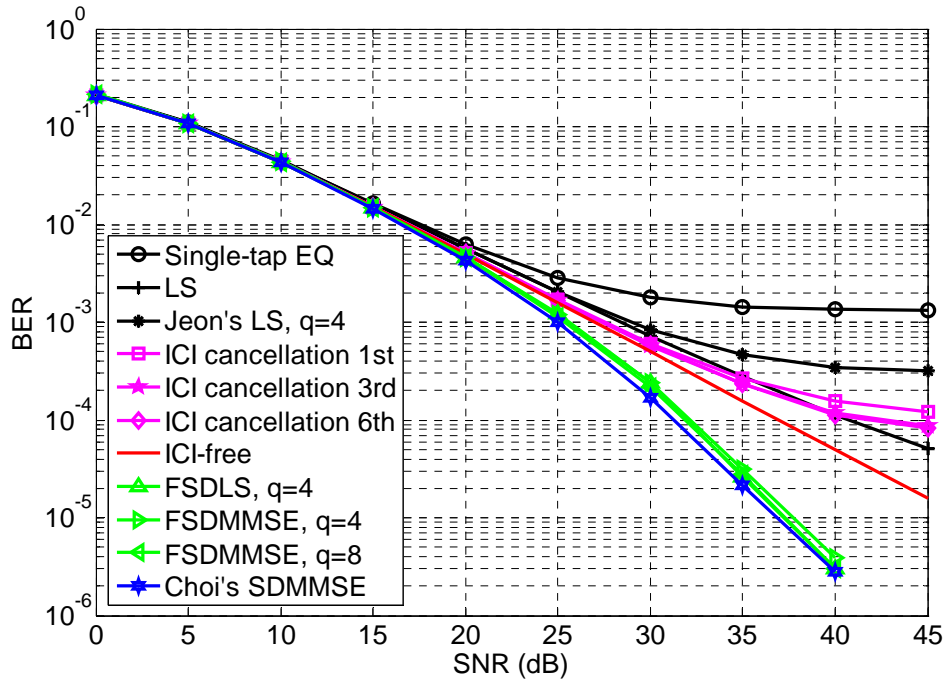


**Figure 5.1** BER performances of the data detection methods in the two-ray equal power channel with  $f_{nd} = 0.040$

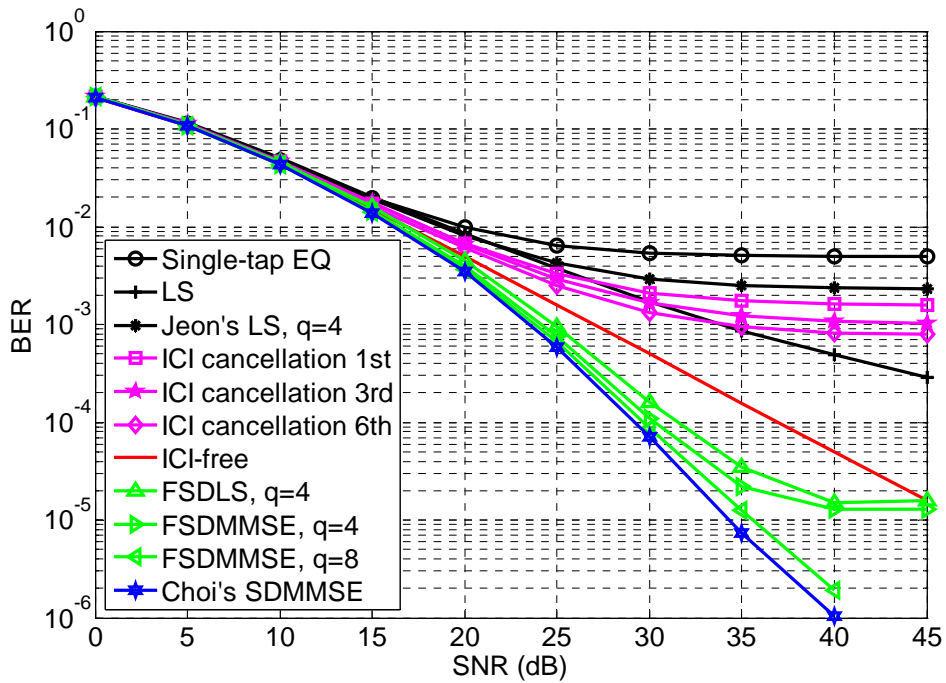


**Figure 5.2** BER performances of the data detection methods in the two-ray equal power channel with  $f_{nd} = 0.083$

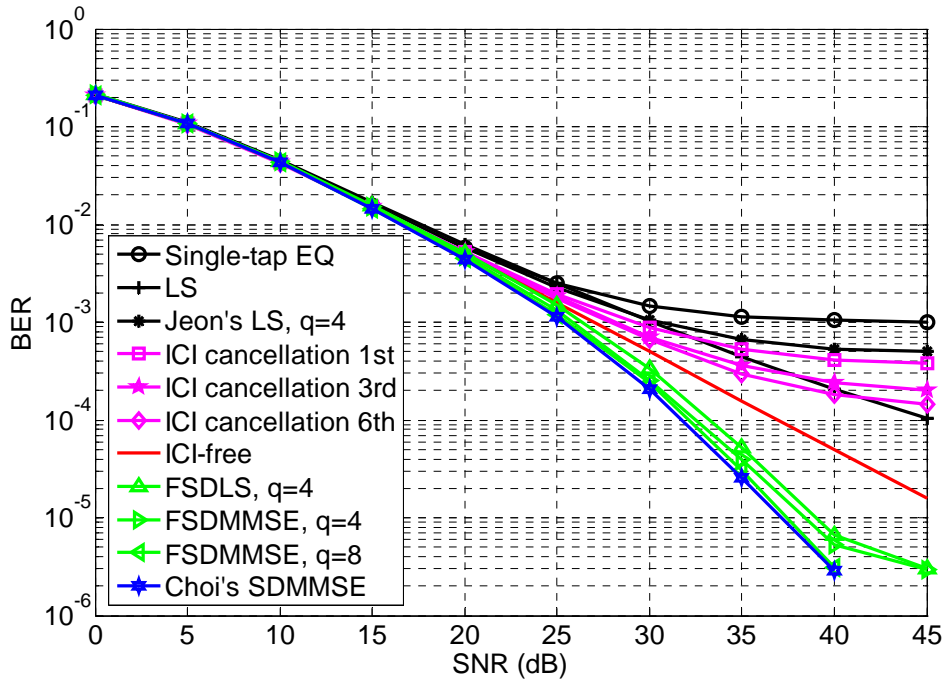


**Figure 5.3** BER performances of the data detection methods in the “Vehicular A” channel with  $f_{nd} = 0.040$

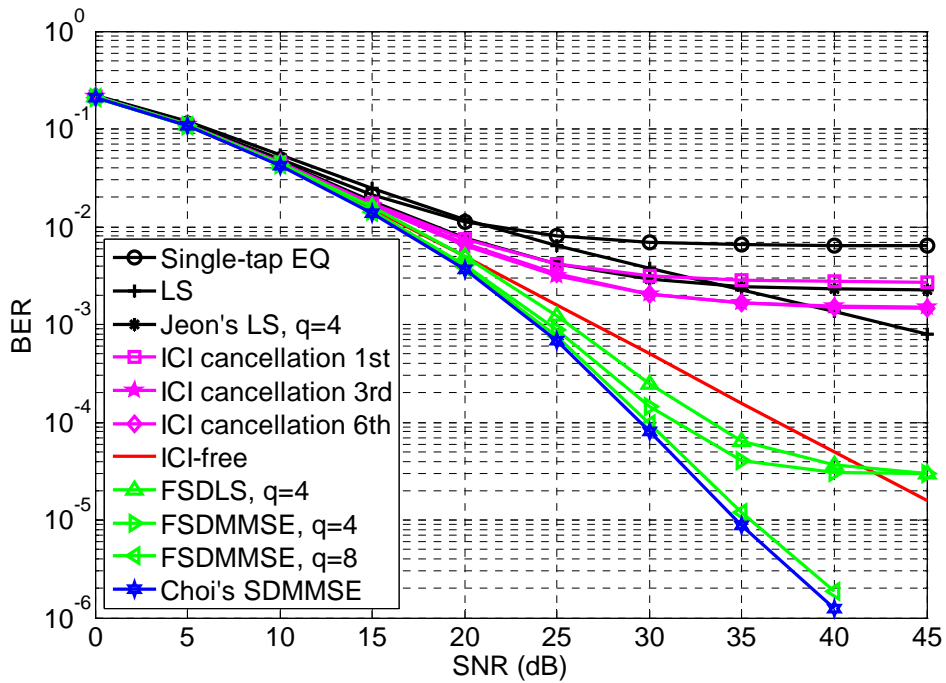


**Figure 5.4** BER performances of the data detection methods in the “Vehicular A” channel with  $f_{nd} = 0.083$

Whether in the 2-ray equal power channel or in the “Vehicular A” channel model, the proposed data detection methods outperform the aforementioned methods except Choi’s method of successive detection because of utilizing time diversity due to the channel variation. Figure 5.1 and Figure 5.3 illustrate the BER performances of the data detection methods in the two channel models with  $f_{nd} = 0.040$ , respectively. Figure 5.1 and Figure 5.3 show that only the 4 most dominant ICI terms closest to the modulated signal in each subchannel, i.e.  $q = 4$ , are needed for the proposed methods and that the proposed method with LS detection is good enough in the fading channels with  $f_{nd} = 0.040$ . There is about 2~3dB performance loss compared to Choi’s method of successive detection with MMSE detection in the SNR range from 20 dB to 40 dB. It is noted that the demodulated signal and its whole ICI terms must be used for interference cancellation in Step P-4. Otherwise, the error floor appears early, and the performance is the same as that of ICI cancellation method.

Figure 5.2 and Figure 5.4 illustrate the BER performances of the detection methods in the two channel models with  $f_{nd} = 0.083$ . In Figure 5.2 and Figure 5.4, the error floor appears for the BER performances of the proposed data detection methods with  $q = 4$  when SNR is up to 35dB. This is because the power of the ignored ICI terms is still large so that ICI terms cannot be effectively suppressed by the block LS or MMSE detection. The error propagation problem becomes severe. Therefore, the considered dominant ICI terms adjacent to the modulated signal in each subchannel must be further increased. The proposed data detection method with MMSE detection and  $q = 8$  is a good choice for OFDM systems in the fading channels with  $f_{nd} = 0.083$ . There is about 0.5~1dB SNR loss compared to Choi’s method of successive detection with MMSE detection in the SNR range from 33 dB to 40 dB.

In conclusion, the proposed methods of successive detection still obtain time diversity even though performing in the frequency domain. As long as the considered

dominant ICI terms adjacent to the modulated signal in each subchannel applied to the proposed methods is enough, the proposed methods almost have the same performances as Choi's method of successive detection.

Next, consider the BER performances of the proposed methods in different detection layers and different subcarriers. Figure 5.5 illustrate the BER performances of the proposed methods in different detection layers in the "Vehicular A" channel model with  $f_{nd} = 0.083$ . Figure 5.6 illustrate the BER performances of the proposed methods with different subcarriers in the "Vehicular A" channel model with  $f_{nd} = 0.083$ . The term "avg" indicates the average BER performance of the proposed method, i.e. the "FSDMMSE,  $q = 8$ " in Figure 5.4. The ordinal numbers indicate the layer numbers of the proposed method. The terms "sc+number" indicate the subcarrier indices. Due to the effect of the frequency-selective fading channel, the signals transmitted in different subcarriers suffer different fading responses. Thus, the previous detection layers have better performances than the succeeding detection layers. Fortunately, the frequency responses change symbol-by-symbol. Therefore, the performances of different subcarriers are almost the same as the average performance.

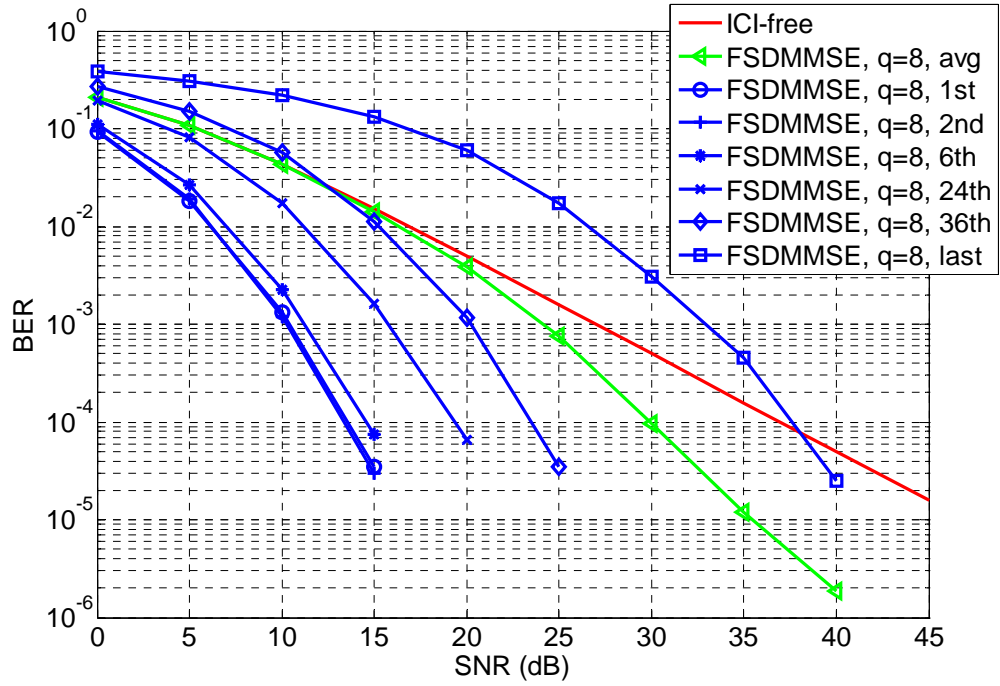


Figure 5.5 BER performances of the proposed method in different detection layers in the “Vehicular A” channel with  $f_{nd} = 0.083$

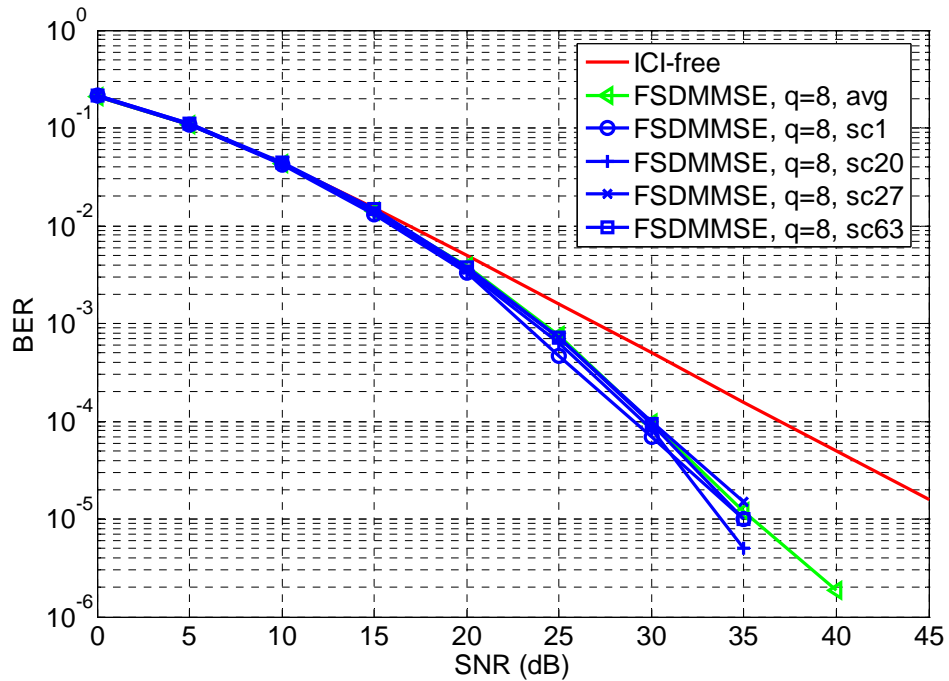


Figure 5.6 BER performances of the proposed method in different subcarriers in the “Vehicular A” channel with  $f_{nd} = 0.083$

## 5.2 The Effect of Channel Estimation Error of the Proposed Frequency-domain Successive Detection Methods

In the above analysis, perfect channel state information is assumed in the detection. However, channel estimation errors occur in practical systems. In order to evaluate the effect of channel mismatches, a complex Gaussian variable  $\varepsilon$  with zero mean representing the estimation error is added to the perfect channel state information for modeling the estimated channel response. The normalized mean square error is defined as

$$\eta = E[|\varepsilon|^2] / P_{ch} \times 100\% \quad (5.1)$$

where  $P_{ch}$  is the channel power and  $E[\ ]$  is the expected-value operator. In the following simulations, EISI “Vehicular A” is considered.

First, the proposed data detection method with  $q = 8$  and the ICI cancellation with 3 detection iterations are investigated for the effect of the channel estimation error. Figure 5.7 shows that the proposed data detection method is more sensitive to the channel estimation error than ICI cancellation method with 3 detection iterations especially when SNR is high. The same result is also observed in Figure 5.8, where  $f_{nd} = 0.083$ . Therefore, there is no gain when the proposed data detection methods are applied in the system with large channel estimation error, especially in the case of small normalized Doppler frequency,  $f_{nd}$ . It implies that reliable channel estimation is necessary for the proposed data detection methods.

Figure 5.9 and Figure 5.10 show how the channel estimation error affects the performances of the proposed data detection methods with different  $q$ 's. In Figure 5.9, the performance losses of the two proposed data detection methods are almost the same when  $f_{nd} = 0.040$ . However, the channel estimation error severely impacts the proposed data detection method with large  $q$  especially when  $f_{nd}$  is high and SNR is

high.

Figure 5.11 illustrates the benefit of the time diversity and the effect of the channel estimation error, particularly. Figure 5.11 shows that the normalized mean square error  $\eta$  must be less than 0.02% for utilizing the time diversity effectively for the proposed data detection method with  $q = 8$  when  $f_{nd} = 0.083$  and SNR = 35dB. The preciseness requirements of the channel estimation for the other tested cases are even more serious.





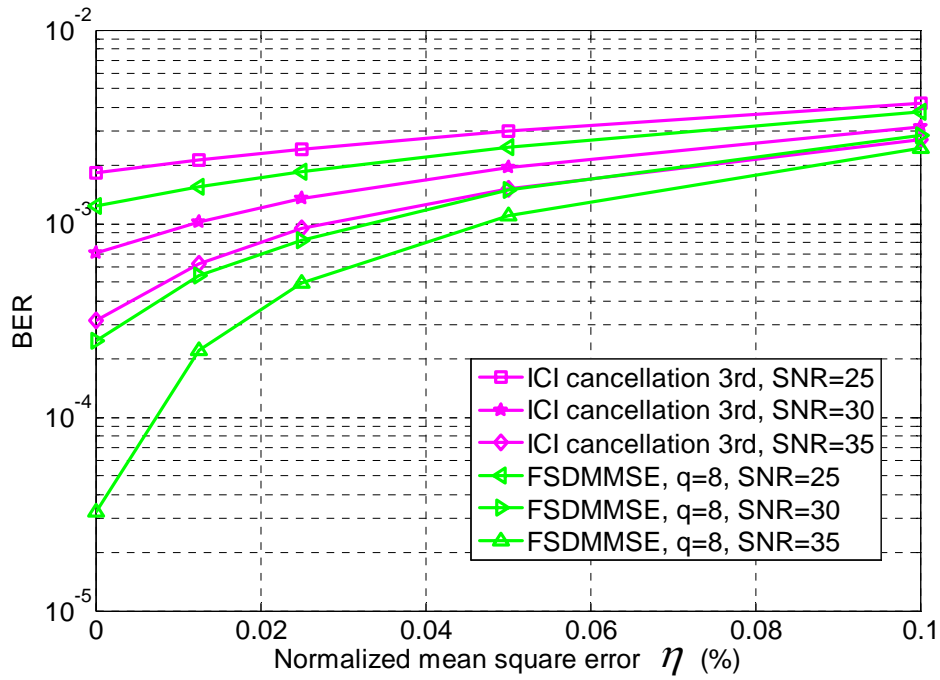


Figure 5.7 BER performances of the detection methods for  $f_{nd} = 0.040$  versus normalized mean square error  $\eta$

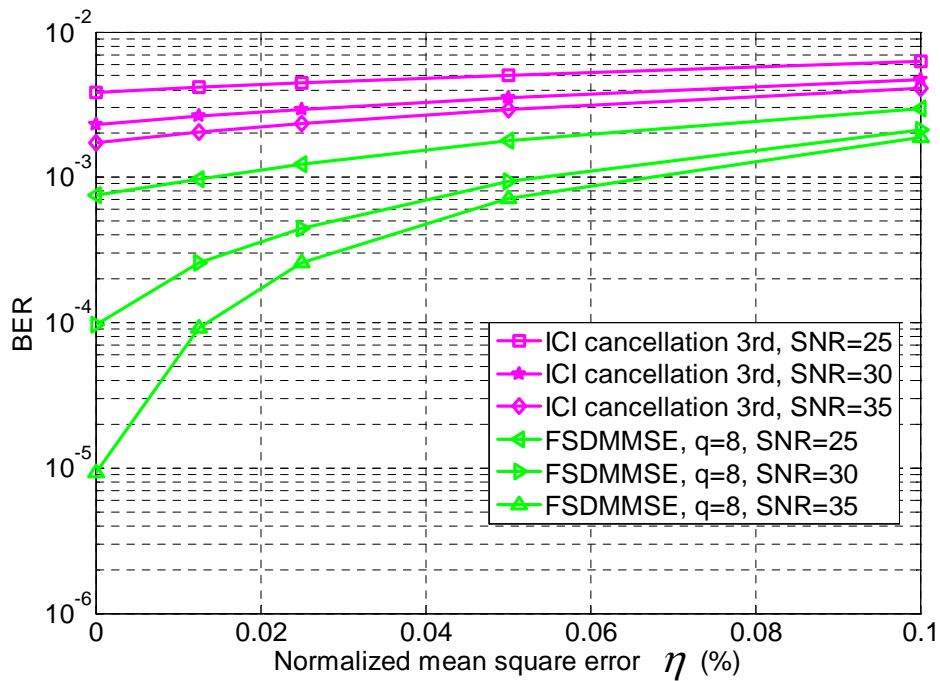
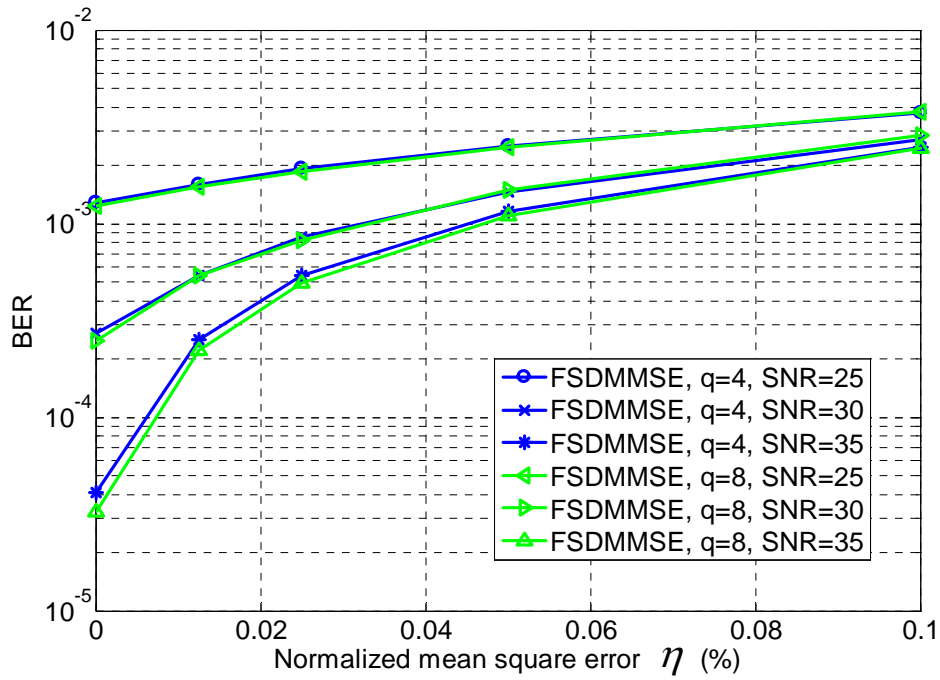
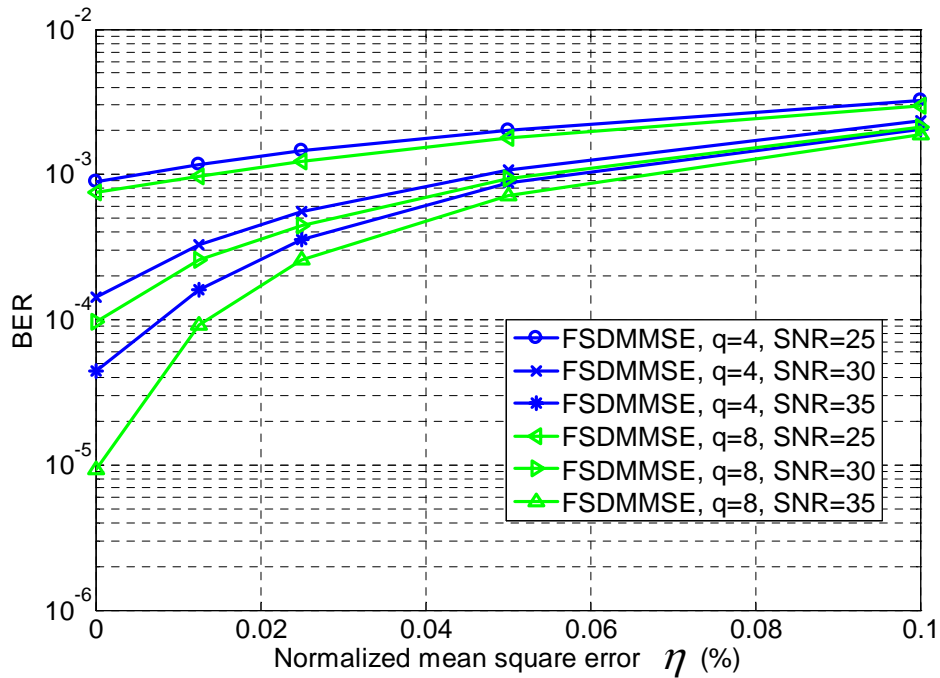


Figure 5.8 BER performances of the detection methods for  $f_{nd} = 0.083$  versus normalized mean square error  $\eta$



**Figure 5.9** BER performances of the proposed detection methods for  $f_{nd} = 0.040$  versus normalized mean square error  $\eta$



**Figure 5.10** BER performances of the proposed detection methods for  $f_{nd} = 0.083$  versus normalized mean square error  $\eta$

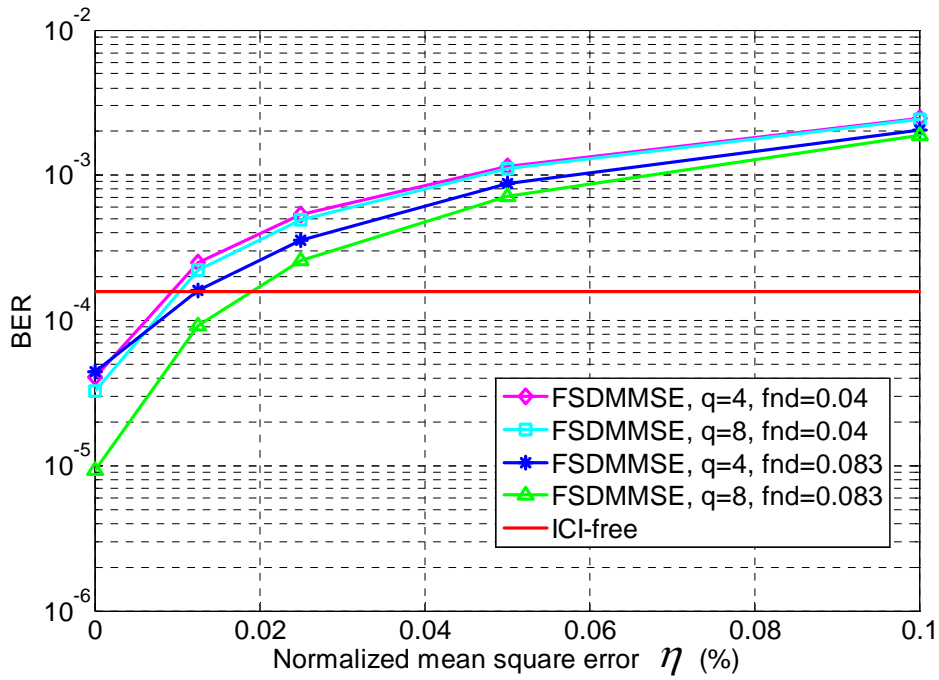


**Figure 5.11** BER performances of the proposed detection methods for different normalized Doppler frequencies  $f_{nd}$ 's versus normalized mean square error  $\eta$  in SNR= 35

## 5.3 The Performances of the Proposed Channel Estimation

### Methods

In this section, the performances of the proposed channel estimation methods are evaluated by computer simulations. In the following simulations, EISI “Vehicular A” is considered. The 16 pilot subcarriers are equispaced along frequency direction, i.e. the indices of the pilot subcarriers are  $\{0, 4, 8, 12, 16, 20, 24, 28, 32, 36, 40, 44, 48, 52, 56, 60\}$  within 64 subcarriers. An all-pilot preamble is attached in front of the data symbols. It is assumed that the maximum path delay time is known at the receiver and that synchronization is perfect.

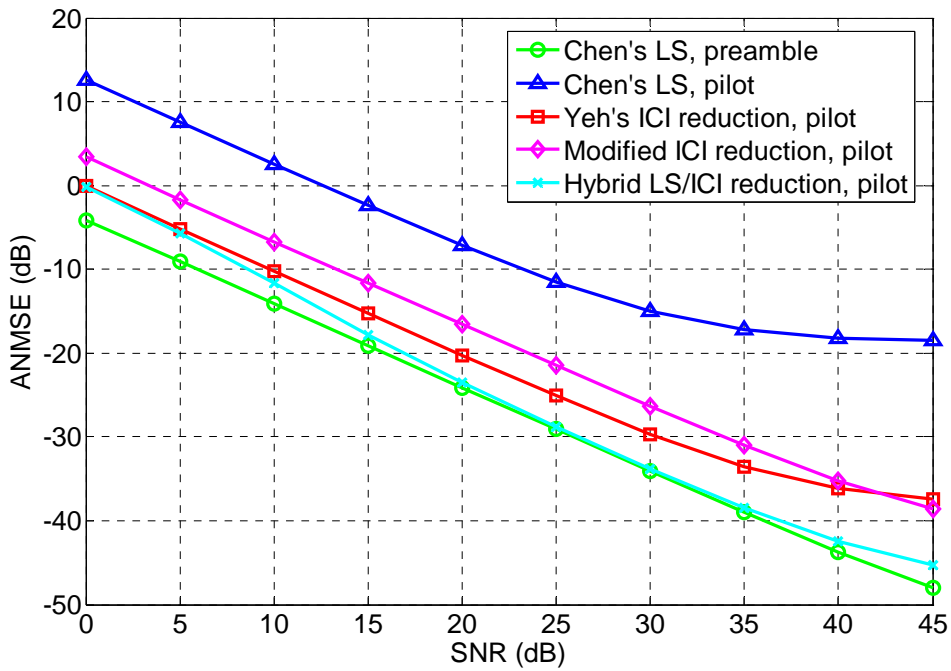


**Figure 5.12** ANMSE performances of the channel estimation methods in the “Vehicular A” channel with  $f_{nd} = 0.040$

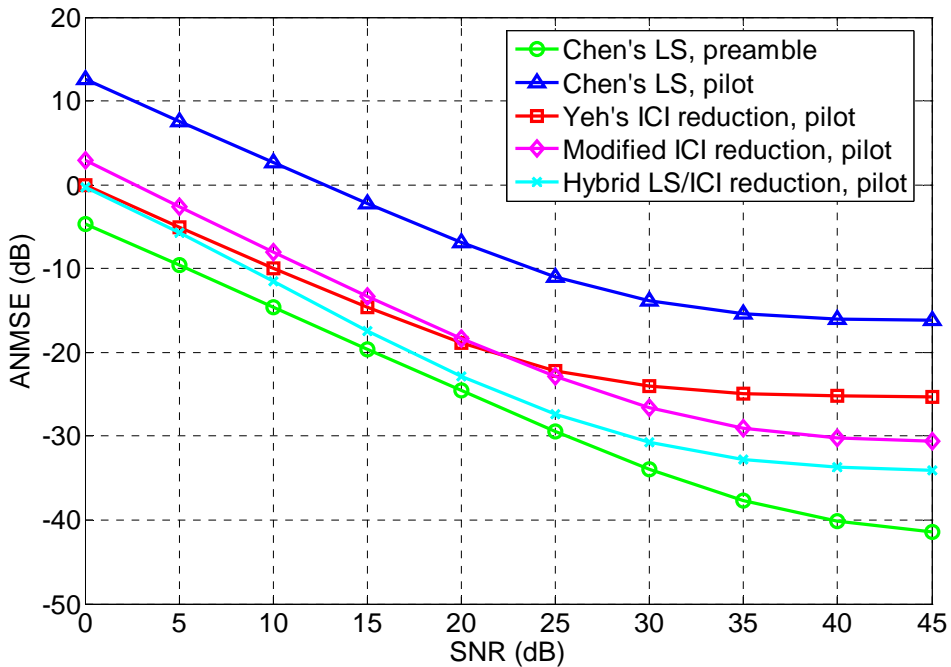


**Figure 5.13** ANMSE performances of the channel estimation methods in the “Vehicular A” channel with  $f_{nd} = 0.083$

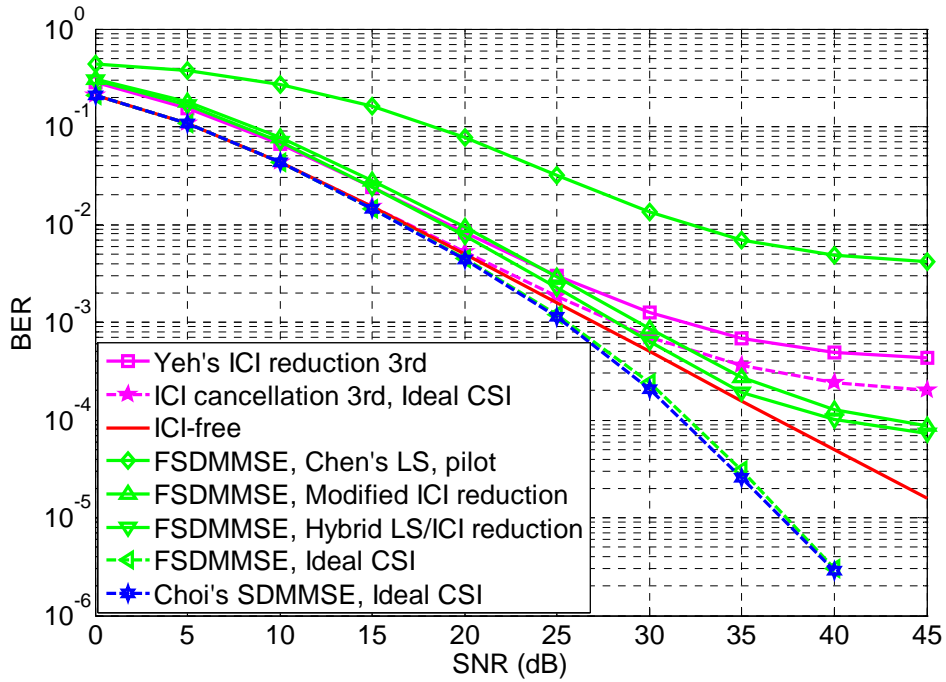


**Figure 5.14** BER performances of the channel estimation methods combined with data detection methods in the “Vehicular A” channel with  $f_{nd} = 0.040$

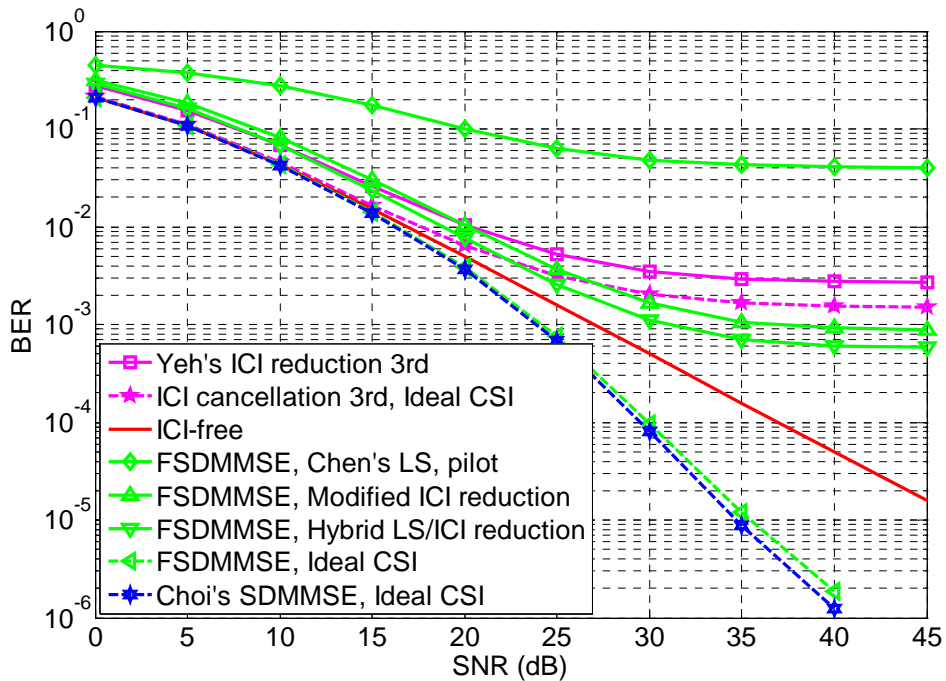


**Figure 5.15** BER performances of the channel estimation methods combined with data detection methods in the “Vehicular A” channel with  $f_{nd} = 0.083$

In Figure 5.12 and Figure 5.13, the terms “Chen’s LS, preamble” and “Chen’s LS, pilot” indicate that Chen’s method of LS channel estimation, introduced in Section 3.2.3, are applied to the all-pilot preamble and the pilot subcarriers, respectively. The term “Yeh’s ICI reduction, pilot” indicates that Yeh’s algorithm of ICI reduction method [11] with 3 detection iterations, introduced in Section 3.2.4, is applied to the pilot subcarriers. The term “Modified ICI reduction” indicates the proposed modification of Yeh’s ICI-reduction method with 3 detection iterations, introduced in Section 4.2.1. The term “Hybrid LS/ICI reduction” indicates the proposed hybrid LS/ICI-reduction channel estimation method, introduced in Section 4.2.2.

In Figure 5.14 and Figure 5.15, the term “ICI-free” indicates the theoretical BER performance of the coherent detection in the time-invariant flat Rayleigh fading channel for the reference of the ICI-free case. The ordinal number appended to “ICI cancellation” and “Yeh’s ICI reduction” indicates the number of the iterations performed in the two methods. The terms “FSDMMSE” and “Choi’s SDMMSE” indicate that the proposed frequency-domain successive detection method with MMSE detection (see Section 4.1) and Choi’s method of successive detection with MMSE detection [7] are adopted in data detection, respectively. The term “Ideal CSI” indicates that ideal channel state information is applied to data detection.

Figure 5.12 and Figure 5.13 illustrate ANMSE performances of the channel estimation methods in the “Vehicular A” channel with  $f_{nd} = 0.040$ , and  $f_{nd} = 0.083$ , respectively. The channel estimation error of the proposed modification of Yeh’s ICI-reduction method with 3 detection iterations is less than that of Yeh’s ICI-reduction method when  $f_{nd} = 0.083$ . However, this benefit is only obtained in high SNR case. This is because the estimated slope of the channel tap,  $\hat{\alpha}_l^i$ , obtained by  $\hat{h}_{ave}^i(l)$  and  $\hat{h}^{i-1}(N-1, l)$  in Figure 4.2 suffer from more noise effect than that

obtained by  $\hat{h}_{ave}^i(l)$  and  $\hat{h}_{ave}^{i-1}(l)$  in Figure 3.6. In other words, it means that the variance of the estimated slope of the channel tap,  $\hat{\alpha}_l^i$ , is large when the distance between the two reference points with noise is small. It will induce large estimation error. Besides, since ICI terms can not be cancelled perfectly in the ICI cancellation procedure of Yeh's method, the channel estimation error increase as  $f_{nd}$  becomes large.

Figure 5.14 and Figure 5.15 illustrate the BER performances of the channel estimation methods combined with data detection methods in the "Vehicular A" channel with  $f_{nd} = 0.040$ , and  $f_{nd} = 0.083$ , respectively. The proposed hybrid LS/ICI-reduction channel estimation method has the best performance of all. The performance loss of the proposed modification of Yeh's ICI reduction method is about 1~3dB in the SNR range from 10 dB to 30 dB when comparing to the proposed hybrid LS/ICI-reduction channel estimation method. Although the two proposed methods outperform Yeh's ICI-reduction method and ICI cancellation method with 3 detection iterations, they still suffer severe ICI effect. There is still large performance loss compared to the proposed frequency-domain successive detection method with ideal channel state information.

By comparison of the simulation results in the previous section (see Figure 5.11), the normalized mean square error  $\eta$  of the channel estimation must be less than 0.02%, i.e. ANMSE must be less than -37dB, for utilizing the time diversity effectively for the proposed data detection methods with  $q = 8$  when  $f_{nd} = 0.083$  and SNR = 35dB. However, Figure 5.13 shows that the two proposed channel estimation methods do not satisfy the preciseness requirements of the proposed data detection methods.

# Chapter 6

## Conclusion



In this thesis, efficient frequency-domain successive detection methods for OFDM systems in fast fading channels are proposed. By evaluating the proposed methods in terms of computational complexities and BER performances, it shows that they operate well in the targeted channel environments and their computational complexities are much less than those of the conventional successive detection. However, their computational complexities are still larger than those of the ICI cancellation methods. Thus, it is a challenging task to find out an adaptive strategy to switch between the low-complexity methods and the proposed methods dynamically according to transmission environments, or to lower the computational complexities of the proposed methods.

Unfortunately, the tolerated channel estimation error of the proposed detection methods is very small according to the simulation results. Thus, existing common channel estimation methods are not good enough for the proposed detection methods.



To make the coherent detection feasible, some channel estimation methods are proposed. The simulation results show that the proposed channel estimation methods outperform the existing common channel estimation methods but do not satisfy the preciseness requirements of the proposed detection methods. Thus, it is still a quite challenging task for future research.

Multiple input multiple output (MIMO) techniques [15] [26] are widely adopted in the next generation communication systems. Thus, data detection and channel estimation for MIMO-OFDM systems in fast fading channels is an original research topic. In these systems, not only ICI but also inter-antenna interference (IAI) will be induced. The main goal is to find out an efficient strategy to suppress the interference and extract the desired signal. With belief, the concepts of the proposed methods can also be applied to these systems.



# Bibliography

- [1] R. W. Chang, "Synthesis of Band Limited Orthogonal Signals for Multichannel Data Transmission," *Bell System Technical Journal*, vol. 45, pp. 1775-1796, Dec. 1966.
- [2] B. R. Saltzberg, "Performance of an efficient parallel data transmission system," *IEEE Transaction on Communications*, vol. COM-15, pp. 805-811, Dec. 1967.
- [3] S. B. Weinstein and P. M. Ebert, "Data transmission by frequency-division multiplexing using the discrete Fourier transform," *IEEE Transaction on Communications*, vol. COM-19, pp. 628-634, Oct. 1971.
- [4] J. Li and M. Kavehrad, "Effect of Time Selective Multipath Fading on OFDM Systems for Broadband Mobile Application," *IEEE Communications Letters*, vol. 3, no. 12, pp. 332-334, Dec. 1999.
- [5] M. Russell and G. L. Stuber, "Interchannel Interference Analysis of OFDM in a Mobile Environment," *Proceedings of Vehicular Technology Conference, 1995 IEEE 45-th*, pp. 820-824, July, 1995.
- [6] S. Chen and T. Yao, "Intercarrier Interference Suppression and Channel Estimation for OFDM Systems in Time-varying Frequency-selective Fading Channels," *IEEE Transactions on Consumer Electronics*, vol. 50, no. 2, pp. 429-435, May 2004
- [7] Y. S. Choi, P.J. Voltz, and F. A. Cassara, "On Channel Estimation and Detection for Multicarrier Signals in Fast and Selective Rayleigh Fading Channels," *IEEE Transaction on Communications*, vol. 49, no. 8, pp.1375-1387, Aug. 2001
- [8] W. G. Jeon, K. H. Chang, and Y. S. Cho, "An Equalization Technique for Orthogonal Frequency-Division Multiplexing Systems in Time-Variant Multipath Channels," *IEEE Transactions on Communications*, vol. 47, no.1, pp.27-32,

Jan. 1999

- [9] Y. R. Zheng, and C. Xiao, "Simulation Models With Correct Statistical Properties for Rayleigh Fading Channels," *IEEE Transactions on Communications*, vol. 51, no. 6, pp. 920-928, June, 2003.
- [10] W. C. Jakes, *Microwave Mobile Communications*. Piscataway, NJ: IEEE Press, 1994
- [11] Y.-H. Yeh, "Design of Pilot-Symbol-Aided Channel Estimation and Equalization for OFDM Systems," M.S. thesis, Institute of Electronics, National Chiao Tung University, Hsin-Chu, Taiwan, 2003.
- [12] IEEE 802.20-PD-06, "Draft 802.20 Permanent Document <System Requirements for IEEE 802.20 Mobile Broadband Wireless Access Systems – Version 14>," IEEE, July 16, 2004.
- [13] Y. Zhao and A. Huang, "A Novel Channel Estimation Method for OFDM Mobile Communication Systems Based on Pilot Signals and Transform-Domain Processing," *Proceedings of Vehicular Technology Conference, 1997 IEEE 47th*, vol. 3, pp. 2089-2094, 1997.
- [14] B. Yang, K. B. Letaief, R. S. Cheng, and Z. Cao, "Windowed DFT Based Pilot-Symbol-Aided Channel Estimation for OFDM Systems in Multipath Fading Channels," *Proceedings of Vehicular Technology Conference, 2000. VTC 2000-Spring Tokyo. 2000 IEEE 51st*, vol. 2, pp.1480-1484, 2000.
- [15] P. W. Wolniansky, G. J. Foschini, G. D. Golden, and R. A. Valenzuela, "V-BLAST: An Architecture for Realizing Very High Data Rates Over the Rich-Scattering Wireless Channel," in *Proc. IEEE ISSSE-98*, pp. 295-300, Sep. 1998.
- [16] G. H. Golub and C. F. V. Loan, *Matrix Computations*, the Johns Hopkins University Press, 1989.

- [17] ETSI TR 101 112 V3.2.0, “Universal Mobile Telecommunications System (UMTS); Selection Procedures for the Choice of Radio Transmission Technologies of the UMTS (UMTS 30.03 version 3.2.0),” ETSI, Apr. 1998.
- [18] Y. Mostofi and D. C. Cox, “ICI Mitigation for Pilot-Aided OFDM Mobile Systems,” *IEEE Transactions on Wireless Communications*, vol. 4, no. 2, pp. 765-774, Mar. 2005
- [19] H. Anton, and C. Rorres, Elementary Linear Algebra. John Wiley & Sons, Inc. 2000.
- [20] S. Chen, G. Dai, and T. Yao, “Zero-forcing Equalization for OFDM Systems over Doubly-selective Fading Channels Using Frequency Domain Redundancy,” *IEEE Transactions on Consumer Electronics*, vol. 50, no. 4, pp.1004-1008, Nov. 2004.
- [21] A. Stamoulis, S. N. Diggavi, and N. Al-Dhahir, “Intercarrier Interference in MIMO OFDM,” *IEEE Transactions on Signal Processing*, vol. 50, no. 10, pp. 2451-2464, Oct. 2002.
- [22] W.-S. Hou and B.-S. Chen, “ICI Cancellation for OFDM Communication Systems in Time-Varying Multipath Fading Channels,” *IEEE Transactions on Wireless Communications*, vol. 4, no. 5, pp. 2100-2110, Sep. 2005.
- [23] S. Tomasin, A. Gorokhov, H. Yang, and J.-P. Linnartz, “Iterative Interference Cancellation and Channel Estimation for Mobile OFDM,” *IEEE Transaction on Wireless Communications*, vol. 4, no. 1, pp.238-245. Jan. 2005.
- [24] Y. Qiao, S. Yu, P. Su, and L. Zhang, “Research on an Iterative Algorithm of LS Channel Estimation in MIMO OFDM Systems,” *IEEE Transactions on Broadcasting*, vol. 51, no. 1, pp. 149-153. Mar. 2005.
- [25] J. Ahn and H. S. Lee, “Frequency domain equalization of OFDM signals over frequency nonselective Rayleigh fading channels,” *Electronics Letters*, vol. 29,

no. 16, pp. 1476-1477, Aug. 1993.

- [26] G. G. Raleigh and J. M. Cioffi, "Spatio-temporal Coding for Wireless communication," *IEEE Transaction on Communications*, vol. 46, no. 3, pp. 357-366, Mar. 1998.
- [27] Y.-H. Yeh, and S.-G. Chen "Reduction of Doppler-induced ICI by interference prediction," *IEEE PIMRC 2004. 15th IEEE international Symposium*, vol. 1, pp. 653-657, Sept. 2004.





# Autobiography

蔡金融，1982年2月6日出生於台北市。2004年自國立交通大學電信工程學系畢業，隨即進入國立交通大學電子工程研究所攻讀碩士學位，致力於訊號處理與通訊系統研究。論文題目是正交分頻多工通信系統於時變與多重路徑衰減通道之通道估測與訊號偵測設計。

